

Quantum Error Correction Exploiting Degeneracy to Approach the Hashing Bound

Kenta Kasai
 Institution of Science Tokyo
 Email: kenta@ict.eng.isct.ac.jp

Abstract

Quantum error correction is essential for realizing scalable quantum computation. Among various approaches, low-density parity-check codes over higher-order Galois fields have shown promising performance due to their structured sparsity and compatibility with iterative decoding algorithms whose computational complexity scales linearly with the number of physical qubits. In this work, we demonstrate that explicitly exploiting the degeneracy of quantum errors—i.e., the non-uniqueness of syndrome representatives—can significantly enhance the decoding performance. Simulation results over the depolarizing channel indicate that the proposed method, at a coding rate of 1/3, achieves a frame error rate as low as 10^{-4} at a physical error rate of 9.45% for a code with 104,000 logical qubits and 312,000 physical qubits, approaching the quantum hashing bound. These findings highlight the critical role of degeneracy in closing the gap to the fundamental limits of quantum error correction.

Index Terms

quantum error correction, low-density parity-check codes, degeneracy

I Introduction

Quantum error correction is a cornerstone for realizing fault-tolerant quantum computation, protecting quantum information from the inevitable decoherence and operational errors encountered in quantum hardware [1],[2]. Since Shor introduced the first quantum error-correcting codes in 1995, extensive research has led to various code families, including stabilizer codes [3], topological codes [4],[5], and concatenated codes [6].

Among these, surface codes, introduced by Kitaev in the late 1990s [4], have emerged as particularly promising candidates due to their local structure and high error-correction thresholds. Surface codes have demonstrated error thresholds approaching 1% under realistic noise models [7],[8], making them a leading architecture for scalable quantum computing. However, a major drawback of surface codes is their inherently low coding rate, typically near zero, which significantly increases the required number of physical qubits and associated hardware overhead.

To address the issue of low coding rates, quantum low-density parity-check (LDPC) codes have attracted considerable attention over the past two decades. Originally developed in classical coding theory by Gallager in 1962 [9], LDPC codes were reintroduced and extensively studied in the 1990s due to their near-capacity performance and efficient iterative decoding algorithms [10],[11]. Quantum LDPC codes were subsequently proposed as stabilizer codes characterized by sparse parity-check matrices, inheriting the classical advantages of efficient decoding [12],[13].

Understanding and improving the minimum distance of quantum LDPC codes is a central challenge in quantum error correction. Early constructions such as hypergraph product codes [14] guaranteed a minimum distance that scales only as $O(\sqrt{n})$, which limits their ability to suppress logical errors at low physical error rates. Recent breakthroughs have demonstrated that it is possible to construct quantum LDPC codes with both linear minimum distance and efficient decoding. In particular, Panteleev and Kalachev [15] introduced a family of quantum LDPC codes with asymptotically good parameters, achieving minimum distance $\Omega(n)$ and constant rate while maintaining low-density parity-check structure. Building upon this, Hastings [16] and Breuckmann and Eberhardt [17] independently proposed similar constructions, further establishing the possibility of good quantum LDPC codes. These advances mark a significant step toward scalable quantum error correction, narrowing the gap between quantum and classical coding theory.

Sparse-graph codes with non-vanishing rate have shown that minimum distance alone is insufficient to fully characterize their practical performance [18, Section 13.8], [12, Section 3.B], and [19, Example 1.18]. Iterative probabilistic decoding algorithms, such as belief propagation (BP), can achieve reliable error correction by effectively exploiting the structural sparsity of these codes. These algorithms perform well even in parameter regimes where conventional minimum-distance-based evaluations would predict failure. Therefore, assessing codes solely by their minimum distance overlooks key factors such as graph structure and decoder interaction—both of which are crucial for achieving near-capacity performance with practical decoding complexity.

Classical LDPC codes are known to scale well with increasing block length, naturally exhibiting good scalability [20]. In contrast, quantum LDPC codes have faced significant challenges in operating at non-vanishing constant rates with long block lengths. This difficulty has largely been attributed to the presence of degeneracy, as well as to the stringent

constraints imposed on the Tanner graph by the orthogonality condition. Both factors interfere with the convergence of BP decoding and suppress the threshold behavior.

To improve the performance of BP decoding in quantum LDPC codes, various techniques have been developed. One approach combines BP with ordered statistics decoding (BP+OSD) [21], which significantly enhances decoding accuracy at the expense of increased complexity [22]. Another approach focuses on identifying and mitigating trapping sets-small harmful substructures in the Tanner graph that lead to decoder failure-enabling targeted remedies to reduce the error floor [23], [24]. More recently, Yao et al. [25] proposed a guided-decimation decoder, where variable nodes are sequentially fixed based on BP likelihoods, and demonstrated that this method achieves performance comparable to BP+OSD while avoiding costly matrix inversions or stabilizer inactivation. Another notable line of work by Miao et al. [26] proposes a code construction method that eliminates length-4 cycles in the joint Tanner graph, thereby mitigating short-cycle-induced decoding failures and improving BP convergence.

Another major advancement is the development of non-binary quantum LDPC codes over higher-order finite fields, motivated by the superior decoding performance observed in classical non-binary LDPC codes [27], [28], [29]. While binary LDPC codes typically exhibit optimal performance with column weight three, non-binary LDPC codes achieve their best performance with column weight two. Leveraging this property, Kasai et al. [30] introduced quantum LDPC codes constructed from circulant permutation matrices (CPMs), using non-binary LDPC codes with column weight two as the underlying structure. This construction demonstrated both improved decoding performance and enhanced structural flexibility. Building upon this approach, Komoto and Kasai [31] further generalized the methodology by proposing a systematic framework based on *affine permutation matrices* (APMs), thereby enabling greater design freedom and decoding robustness. It should be noted that although the quantum error-correcting codes proposed in [30], [31] are constructed using non-binary LDPC codes, the resulting quantum codes are ultimately binary CSS codes.

Non-binary LDPC codes can be implemented efficiently and cost-effectively on GPUs, making real-time decoding feasible [32]. Recent advances include implementations of FFT-based sum-product or min-max algorithms over \mathbb{F}_q on modern GPU architectures, achieving throughputs in the multi-gigabit range. For example, a GPU-accelerated min-max decoder achieved approximately 1.4 Gbps [32], while a layered-min-sum implementation on RTX4090 delivered up to 27 Gbps for long block-length codes [33].

The high-rate codes (with row weight $L \geq 8$ and rate $R \geq 1/2$) proposed in [31] achieve a sharp threshold using joint BP alone (see Figure 2). Experimental results demonstrate an exponential decrease in error rates as the block length increases. However, as the code length increases and the rate decreases, these codes exhibit more pronounced error-floor behavior in the frame error rate (FER) curves at low noise levels (see Figure 2). This error floor is attributed to the presence of short cycles in the Tanner graph. For codes with row weight $L = 8$ and rate $R = 1/2$, the issue was addressed in [34] by exploiting the non-commutativity of APMs to develop a modified construction method that eliminates such cycles. As a result, the FER was successfully reduced to 10^{-5} at a physical error rate of $p_D = 6.49\%$ over the depolarizing channel. Notably, this performance approaches the hashing bound for the same rate, which is given by $p_D^* = 7.44\%$.

To enable reliable error correction at even higher noise levels, we focus on codes with row weight $L = 6$ and rate $R = 1/3$, for which the error-floor behavior is more pronounced than in the $L = 8$, $R = 1/2$ case. Our target is to achieve a FER of 10^{-4} . We propose a modified code construction and decoding method to address this issue. Unlike the approach in [22], where joint BP leaves residual errors proportional to the block length, the errors uncorrected by joint BP in our setting are limited to a constant number of bits, independent of the code length. This opens the possibility of correcting them through efficient post-processing. Preliminary results toward this goal were briefly explored in [35], which focused on a specific class of graph structures. In contrast, the present work significantly extends that direction by proposing a new code construction method along with theoretical justification and empirical validation.

This paper presents a new code construction method for quantum error correction based on non-binary LDPC codes, extending the conventional framework [31] with the following key innovations:

- We identify inevitable cycle structures that arise from the orthogonality condition inherent to CSS-type constructions.
- We analyze these cycles and demonstrate that they can be classified into harmful ones that contribute to logical errors and harmless ones that do not.
- We systematically eliminate the harmful short cycles in the Tanner graph by strategically assigning nonzero symbols over higher-order Galois fields.
- We develop a decoding algorithm that explicitly accounts for degeneracy, leading to substantial improvements in decoding performance.
- Simulation results over the depolarizing channel show that the proposed code, with $n = 312,000$ physical qubits, achieves a frame error rate (FER) of 10^{-4} at a physical error rate of $p_D = 9.45\%$, approaching the quantum hashing bound.

Together, these contributions provide a viable pathway toward practical, high-performance quantum error correction by balancing algebraic code design with decoding robustness.

We summarize the notation used throughout this paper as follows. For a natural number n , we define $[n] = \{0, 1, \dots, n - 1\}$. The finite field with q elements is denoted by \mathbb{F}_q , and the ring of integers modulo n is denoted by \mathbb{Z}_n , representing the set of residue classes modulo n . Vectors and one-dimensional arrays are denoted using underlined symbols, such as

$$\underline{x} = (x_0, x_1, \dots, x_{N-1}).$$

Unless otherwise stated, all vectors are treated as column vectors, even when written in row form. To simplify notation, the transpose symbol is omitted wherever possible. Indices for arrays and matrices are assumed to start from zero, unless noted otherwise. Elements of the finite field \mathbb{F}_q are typically denoted using Greek letters such as ξ .

II Permutation Matrices for LDPC Codes

This section provides a foundational framework for understanding how permutation matrices (PMs) are used in the construction of structured LDPC codes, particularly in the quantum setting. We begin by introducing permutation matrices and their algebraic properties, followed by two important subclasses: APMs and CPMs. We then discuss how arrays of PMs can be used to define binary LDPC parity-check matrices and classify such constructions as protograph-based, APM-based, or QC-based codes depending on the permutation class. To analyze the structure of these matrices, we introduce the concept of *block cycles*, define their composite functions, and explain how they relate to the existence of cycles in the Tanner graph. In particular, we focus on totally closed block cycles (TCBCs), which play a central role in determining the upper bound of girth. We conclude the section by presenting an explicit example of a TCBC and a theorem establishing an upper bound on the girth for QC-LDPC codes, motivating the use of non-commutative APMs for our construction.

II-A Permutation Matrices (PMs)

Let P be a positive integer. Define \mathcal{F}_P as the set of all permutations from $[P]$ to itself. The identity permutation is written as id . A permutation $f \in \mathcal{F}_P$ is associated with a binary permutation matrix $F \in \mathbb{F}_2^{P \times P}$ of size P through the rule:

$$f(j) = i \iff F_{i,j} = 1,$$

for $i, j \in [P]$. We denote this correspondence by $f \sim F$, or simply write $f = F$ when the context is clear. With a slight abuse of notation, we will freely switch between viewing f as a permutation and as its associated matrix F .

This correspondence preserves the algebraic structure of permutations in the matrix domain. Let $f, g \in \mathcal{F}_P$ and $F, G \in \mathbb{F}_2^{P \times P}$ with $f \sim F$ and $g \sim G$. Then the composition of permutations corresponds to matrix multiplication: the composed permutation $f \circ g$ satisfies $f \circ g \sim FG$. That is, applying g first and then f is equivalent to multiplying the corresponding permutation matrices G and F (from right to left). We say that two permutations f and g *commute* if $f \circ g = g \circ f$. Furthermore, the inverse of a permutation corresponds to the transpose of its matrix: $f^{-1} \sim F^\top$. This follows from the fact that transposing a permutation matrix swaps its rows and columns, effectively reversing the direction of the permutation.

The following lemma will be used several times later, so we assign it a number for easy reference.

Lemma 1. If f and g commute, then each of the following pairs also commute: f^{-1} and g^{-1} , f and g^{-1} , and f^{-1} and g .

Proof. Suppose $f \circ g = g \circ f$. Then we have

$$f \circ g \circ g^{-1} = g \circ f \circ g^{-1}, \quad \text{so} \quad f = g \circ f \circ g^{-1}.$$

Composing both sides on the left with g^{-1} gives

$$g^{-1} \circ f = f \circ g^{-1}.$$

Thus, f and g^{-1} commute. In the same way, we obtain

$$f^{-1} \circ g = g \circ f^{-1} \quad \text{and} \quad f^{-1} \circ g^{-1} = g^{-1} \circ f^{-1}.$$

□

II-B Affine and Circulant Permutation Matrices

For integers $a, b \in \mathbb{Z}_P$, we define a permutation $f : \mathbb{Z}_P \rightarrow \mathbb{Z}_P$ of the form

$$f(j) = aj + b \pmod{P}.$$

Note that the sets \mathbb{Z}_P and $[P]$ are identical as sets. It is known that $f \in \mathcal{F}$ if and only if $\gcd(a, P) = 1$ [36]. A permutation matrix arising from a permutation of the above form is called an *affine permutation matrix* (APM). In this paper, we identify permutation functions with their corresponding permutation matrices, and hence refer to such matrices as APMs. We denote the set of all such matrices by \mathcal{A}_P . When $a = 1$, the affine permutation reduces to a simple shift: $f(j) = j + b \pmod{P}$. The corresponding permutation matrix is called a *circulant permutation matrix* (CPM), and we denote the set of all such matrices by \mathcal{Q}_P . Any two elements $f, g \in \mathcal{Q}_P$ commute with each other; that is, $f \circ g = g \circ f$ always holds. In contrast, two affine permutations $f, g \in \mathcal{A}_P$ do not necessarily commute.

Example 1. Consider the affine permutation over \mathbb{Z}_5 defined by

$$f(j) = 2j + 1 \pmod{5}.$$

Note that both row and column indices are taken modulo 5. The corresponding permutation matrix $F \in \mathbb{F}_2^{5 \times 5}$ is given by

$$F = \begin{pmatrix} 0 & 0 & 1 & 0 & 0 \\ 1 & 0 & 0 & 0 & 0 \\ 0 & 0 & 0 & 1 & 0 \\ 0 & 1 & 0 & 0 & 0 \\ 0 & 0 & 0 & 0 & 1 \end{pmatrix}.$$

The inverse permutation is given by

$$f^{-1}(i) = 3i + 2 \pmod{5},$$

which can be verified directly by checking that $f \circ f^{-1} = \text{id}$. The inverse permutation corresponds to the transpose of the matrix:

$$F^\top = \begin{pmatrix} 0 & 1 & 0 & 0 & 0 \\ 0 & 0 & 0 & 1 & 0 \\ 1 & 0 & 0 & 0 & 0 \\ 0 & 0 & 1 & 0 & 0 \\ 0 & 0 & 0 & 0 & 1 \end{pmatrix}.$$

□

II-C Low-Density Parity-Check Matrices

We represent the column and row weights by integers $J \geq 2$ and even $L \geq 4$, respectively. Let $\hat{H} = (f_{ij}) \in \mathcal{F}_P^{J \times L}$ be a permutation array whose entries are taken from a set of permutations \mathcal{F}_P . This array can also be interpreted as a binary parity-check matrix in $\hat{H} = (f_{ij}) = (F_{ij}) \in \mathbb{F}_2^{JP \times LP}$. We refer to each $P \times P$ matrix appearing in \hat{H} as a *block*. LDPC codes defined by such parity-check matrices are conventionally referred to as protograph codes, APM-LDPC codes, and quasi-cyclic LDPC (QC-LDPC) codes when the permutations are taken from \mathcal{F}_P , \mathcal{A}_P , and \mathcal{Q}_P , respectively. As an example, see the parity-check matrices \hat{H}_X and \hat{H}_Z in Example 3.

II-D Block Cycles

Let $\hat{H} = (f_{ij})$ be a parity-check matrix, where each $f_{ij} \in \mathcal{F}_P$. We consider a path that moves alternately in horizontal and vertical directions across the blocks of \hat{H} , beginning and ending at the same block. Such a path is represented as

$$\underline{c} := f_{11} \rightarrow f_{12} \rightarrow f_{21} \rightarrow f_{22} \rightarrow \cdots \rightarrow f_{n1} \rightarrow f_{n2} \rightarrow f_{11}$$

within the following submatrix S of \hat{H} :

$$S = \begin{pmatrix} f_{11} & f_{12} & * & * & * & * \\ * & f_{21} & f_{22} & * & * & * \\ * & * & \ddots & \ddots & * & * \\ * & * & * & * & f_{n-1,1} & f_{n-1,2} \\ f_{n2} & * & * & \cdots & * & f_{n1} \end{pmatrix}.$$

In this construction, each step in the path moves either to a different row or to a different column, but not both simultaneously. That is, consecutive blocks must differ in exactly one of their row or column indices. For instance, the column indices of f_{11} and f_{12} must be different, and likewise, the row indices of f_{12} and f_{21} must differ. Such a path \underline{c} is referred to as a *block cycle*.

We define the *composite function* associated with the block cycle as

$$f_{\underline{c}}(j) := (f_{n2}^{-1} f_{n1} \cdots f_{22}^{-1} f_{21} f_{12}^{-1} f_{11})(j),$$

for $j \in \mathbb{Z}_P$, where the composition operator \circ is omitted for simplicity. Equivalently, the inverse function can be written as

$$f_{\underline{c}}^{-1}(j) = (f_{11}^{-1} f_{12} \cdots f_{n1}^{-1} f_{n2})(j), \quad j \in \mathbb{Z}_P.$$

We call the block cycle *closed* if $f_{\underline{c}}(j) = j$ for some $j \in \mathbb{Z}_P$, and *open* otherwise. In particular, if $f_{\underline{c}}(j) = j$ for all $j \in \mathbb{Z}_P$, that is, if $f_{\underline{c}} = \text{id}$, the block cycle is said to be *totally closed*.

For a block cycle \underline{c} in \hat{H} , there are at most P corresponding Tanner cycles in \hat{H} , each denoted by \mathcal{C} . We say that \mathcal{C} is contained in \underline{c} , and write $\underline{c} \in \mathcal{C}$. We use \underline{c} also to denote the set of all such Tanner cycles contained in the block cycle \underline{c} . The existence of a closed block cycle implies the presence of a cycle in the corresponding Tanner graph [36], [37]. Conversely, if no closed block cycle exists, then the Tanner graph contains no cycles. To avoid confusion with block cycles, we explicitly refer to cycles in the Tanner graph as *Tanner cycles* throughout this paper. We define the *girth* of a given parity-check matrix as the length of the shortest closed block cycle contained in it. This length coincides with the length of the shortest cycle in the Tanner graph.

When column weight $J = 2$, each step in the block cycle alternates between the first and second row blocks, and hence its length is always a multiple of 4. In such cases, if we assume that the cycle starts from a block in the upper row and that the first move is in the horizontal direction, the block cycle can be uniquely specified by the sequence of column indices. Moreover, if every element in the first row block appears in a unique column (i.e., no two entries in the same row block share a column), then the entire block cycle can be fully described by the sequence of permutation elements. The following example illustrates a concrete instance of a block cycle and demonstrates how the composite function $f_{\underline{c}}$ is evaluated. In particular, it shows that the cycle is totally closed, thereby providing a constructive example of a totally closed block cycle (TCBC).

Example 2. We consider the following example of a parity-check matrix \hat{H} , which corresponds to the one shown in (4) and illustrated in Example 3.

$$\hat{H}_X = \left(\begin{array}{ccc|cc} f_0 & f_1 & f_2 & g_0 & g_1 & g_2 \\ f_2 & f_0 & f_1 & g_2 & g_0 & g_1 \end{array} \right).$$

Let us consider a block cycle \underline{c} starting from the $(0, 0)$ -th block in the matrix \hat{H} .

$$\underline{c} = \bar{f}_0 \rightarrow \bar{g}_0 \rightarrow g_2 \rightarrow f_0 \rightarrow \bar{f}_1 \rightarrow \bar{g}_2 \rightarrow g_1 \rightarrow f_1 \rightarrow \bar{f}_2 \rightarrow \bar{g}_1 \rightarrow g_0 \rightarrow f_2 \rightarrow \bar{f}_0.$$

where overlined symbols indicate blocks in the upper row. Since the entries in the upper row are distinct, each one determines a unique column index. This traversal can be compactly expressed by the sequence:

$$\underline{c} = f_0 \Rightarrow g_0 \Rightarrow f_1 \Rightarrow g_2 \Rightarrow f_2 \Rightarrow g_1 \Rightarrow f_0.$$

The notation \rightarrow indicates the full sequence of block-level transitions, whereas \Rightarrow is used in the compact form, omitting the intermediate transitions between upper and lower rows. From the values in (5), evaluating the composite function $f_{\underline{c}}$ associated with this block cycle yields $f_{\underline{c}}(x) = x$. Therefore, this example constitutes a TCBC. \square

From the following theorem, it follows that any QC-LDPC code whose parity-check matrix contains commutative submatrices of size at least 2×3 has girth at most 12.

Theorem 1 ([38]). Let $a, b, c, d, e, f \in \mathcal{F}_P$ be mutually commuting elements. In particular, this commutativity condition is automatically satisfied when $a, b, c, d, e, f \in \mathcal{Q}_P$. Consider the following 2×3 subarray of a larger permutation array H :

$$\begin{pmatrix} a & b & c \\ d & e & f \end{pmatrix}.$$

Then, the block cycle of length 12 $\underline{c} := a \Rightarrow b \Rightarrow c \Rightarrow a \Rightarrow b \Rightarrow c \Rightarrow a$ is closed. Moreover, it forms a TCBC.

Proof. Since all the elements commute, the following composition reduces to the identity function:

$$f_{\underline{c}}^{-1} = a^{-1} b e^{-1} f c^{-1} a d^{-1} e b^{-1} c f^{-1} d = \text{id}.$$

Hence, the composite function associated with this block cycle is the identity, confirming that it is a TCBC. \square

This theorem implies that when the permutation array is constructed using mutually commuting blocks such as CPMs, the girth of the Tanner graph is upper bounded by 12. In [34], a novel construction was proposed using APMs that do not necessarily commute. By exploiting this non-commutativity, the authors succeeded in constructing Calderbank–Shor–Steane (CSS) codes whose Tanner graphs achieve girth 16.

III Conventional Construction

In the remainder of this paper, we restrict our attention to the case where the column weight is $J = 2$. In [31], the construction method for CSS codes based on non-binary LDPC codes—originally proposed for \mathcal{Q}_P -valued arrays in [30]—was generalized to support \mathcal{F}_P -valued arrays. This generalized method [31] is referred to as the *conventional construction* in this paper.

Within this framework, we ultimately construct the binary parity-check matrices H_X and H_Z that define a CSS code from two arrays of permutations

$$\underline{f} := (f_0, \dots, f_{L/2-1}) \text{ and } \underline{g} := (g_0, \dots, g_{L/2-1})$$

in $\mathcal{F}_P^{L/2}$. As intermediate steps, we generate auxiliary binary matrices \hat{H}_X and \hat{H}_Z , along with non-binary matrices H_Γ and H_Δ , which are subsequently used in the decoding process. Since this construction serves as the foundation for the proposed code construction presented in Section V, we provide a detailed overview below.

Section III-A describes a construction of orthogonal binary matrix pairs (\hat{H}_X, \hat{H}_Z) . Section III-B explains how to convert these binary matrices into orthogonal \mathbb{F}_q -valued matrix pairs (H_Γ, H_Δ) . Finally, Section III-C presents a construction of binary matrix pairs (H_X, H_Z) that are equivalent to (H_Γ, H_Δ) .

III-A Construction of \hat{H}_X and \hat{H}_Z

The following requirement on \underline{f} and \underline{g} is used to ensure that the resulting matrices \hat{H}_X and \hat{H}_Z are orthogonal [31].

Requirement 1. We require that the following commutativity condition holds:

$$f_{\ell-j} f_{k-\ell} = f_{k-\ell} f_{\ell-j} \quad \text{for all } \ell \in [L/2], j, k \in [J]. \quad (1)$$

Here, the indices of f and g are understood modulo $L/2$. \square

This condition (1) is equivalently expressed by any of the following three statements.

$$f_{\ell-j} g_{k-\ell} = g_{k-\ell} f_{\ell-j} \quad \text{for all } \ell \in [L/2], j, k \in [J], \quad (2)$$

$$f_\ell \text{ commutes with } g_{-\ell+j} \text{ for all } \ell \in [L/2] \text{ and } j \in \{0, \pm 1, \dots, \pm(J-1)\}, \quad (3)$$

$$g_\ell \text{ commutes with } f_{-\ell+j} \text{ for all } \ell \in [L/2] \text{ and } j \in \{0, \pm 1, \dots, \pm(J-1)\}.$$

This commutativity condition guarantees that each pair of corresponding blocks in \hat{H}_X and \hat{H}_Z ensures the orthogonality. As shown in Table I, the table lists the $(\underline{f}, \underline{g})$ pairs for which commutativity is required when $L = 6, 8$ and 10 . A value of “1” indicates that the pair must satisfy the commutativity condition $f_i g_j = g_j f_i$, while “–” denotes that no such requirement is imposed. When $L = 6$, it is known that all f_i and g_j commute.

TABLE I: Commutativity matrices for various values of L with fixed $J = 2$.

(a) $J = 2, L = 6$	(b) $J = 2, L = 8$	(c) $J = 2, L = 10$
$f_0 \mid \begin{array}{ccc} g_0 & g_1 & g_2 \end{array}$	$f_0 \mid \begin{array}{cccc} g_0 & g_1 & g_2 & g_3 \end{array}$	$f_0 \mid \begin{array}{ccccc} g_0 & g_1 & g_2 & g_3 & g_4 \end{array}$
$f_1 \mid \begin{array}{ccc} 1 & 1 & 1 \end{array}$	$f_1 \mid \begin{array}{cccc} 1 & - & 1 & 1 \end{array}$	$f_1 \mid \begin{array}{ccccc} 1 & - & - & 1 & 1 \end{array}$
$f_2 \mid \begin{array}{ccc} 1 & 1 & 1 \end{array}$	$f_2 \mid \begin{array}{cccc} - & 1 & 1 & 1 \end{array}$	$f_2 \mid \begin{array}{ccccc} - & - & 1 & 1 & 1 \end{array}$
	$f_3 \mid \begin{array}{cccc} 1 & 1 & 1 & - \end{array}$	$f_3 \mid \begin{array}{ccccc} - & 1 & 1 & 1 & - \end{array}$
		$f_4 \mid \begin{array}{ccccc} 1 & 1 & 1 & - & - \end{array}$

We show that the matrices \hat{H}_X and \hat{H}_Z , defined below using \underline{f} and \underline{g} that satisfy Requirement 1, are orthogonal; that is, $\hat{H}_X \hat{H}_Z^\top = 0$. Let us begin by defining these matrices.

Definition 1. Construction of \hat{H}_X and \hat{H}_Z Let $f_0, \dots, f_{L/2-1}$ and $g_0, \dots, g_{L/2-1}$ be elements of \mathcal{F}_P , and assume that the indices are extended cyclically, i.e., $f_k = f_{k \bmod (L/2)}$ and similarly for g_k .

We first define the following four types of \mathcal{F}_P -valued arrays of length $L/2$:

$$\begin{aligned} (\hat{H}_X^{(L,j)})_\ell &= f_{\ell-j}, & (\hat{H}_X^{(R,j)})_\ell &= g_{\ell-j}, \\ (\hat{H}_Z^{(L,j)})_\ell &= g_{-(\ell-j)}^{-1}, & (\hat{H}_Z^{(R,j)})_\ell &= f_{-(\ell-j)}^{-1}, \end{aligned}$$

for $j \in [L/2]$ and $\ell \in [L/2]$. The arrays $\hat{H}_X^{(L,j)}$, $\hat{H}_X^{(R,j)}$, $\hat{H}_Z^{(L,j)}$, and $\hat{H}_Z^{(R,j)}$ serve as building blocks for constructing the permutation arrays \hat{H}_X and \hat{H}_Z used in our CSS code.

Next, we define the \mathcal{F}_P -valued $J \times L$ array \hat{H}_X as the horizontal concatenation of the left and right halves:

$$\begin{aligned}\hat{H}_X &\stackrel{\text{def}}{=} (\hat{H}_X^{(\text{L})} \mid \hat{H}_X^{(\text{R})}) \\ &\stackrel{\text{def}}{=} \left(\begin{array}{c|c} \hat{H}_X^{(\text{L},0)} & \hat{H}_X^{(\text{R},0)} \\ \hat{H}_X^{(\text{L},1)} & \hat{H}_X^{(\text{R},1)} \\ \vdots & \vdots \\ \hat{H}_X^{(\text{L},J-1)} & \hat{H}_X^{(\text{R},J-1)} \end{array} \right)\end{aligned}$$

Alternatively, letting $N := LP$ and $M := JP$, the matrix \hat{H}_X can equivalently be regarded as a binary matrix of size $M \times N$. The matrix \hat{H}_Z is defined analogously, using the row vectors $\hat{H}_Z^{(\text{L},j)}$ and $\hat{H}_Z^{(\text{R},j)}$ in place of their X -counterparts. \square

Alternatively, if we define the j -th row of \hat{H}_X for $j \in [J]$ as

$$\hat{H}_X^{(j)} := (\hat{H}_X^{(\text{L},j)} \mid \hat{H}_X^{(\text{R},j)}),$$

then the matrix can be compactly expressed as

$$\hat{H}_X = \left(\begin{array}{c} \hat{H}_X^{(0)} \\ \hat{H}_X^{(1)} \\ \vdots \\ \hat{H}_X^{(J-1)} \end{array} \right).$$

Strictly speaking, the index range $j \in [J]$ is sufficient for the definition of \hat{H}_X . However, we later make use of $\hat{H}_X^{(2)}$, which coincides with $\hat{H}_X^{(L/2-1)}$ due to the $L/2$ -periodicity of the permutation indices f_i and g_j . Therefore, we adopt the extended index range $j \in [L/2]$ in the current definition.

Example 3. Let $P = 8$, $J = 2$, and $L = 6$. Using the APMs or CPMs f_0, \dots, f_2 and g_0, \dots, g_2 specified as follows:

$$\begin{aligned}\underline{f} &= (5X + 7, \quad 5X + 3, \quad 1X + 6), \\ \underline{g} &= (5X + 7, \quad 5X + 5, \quad 5X + 7),\end{aligned}$$

we compute their inverses:

$$\begin{aligned}(f_0^{-1}, \quad f_1^{-1}, \quad f_2^{-1}) &= (5X + 5, \quad 5X + 1, \quad 1X + 2), \\ (g_0^{-1}, \quad g_1^{-1}, \quad g_2^{-1}) &= (5X + 5, \quad 5X + 7, \quad 5X + 5).\end{aligned}$$

Based on these permutations, we define the following $J \times L$ protograph-based permutation array \hat{H}_X :

$$\begin{aligned}\hat{H}_X &= \left(\begin{array}{ccc|cc} f_0 & f_1 & f_2 & g_0 & g_1 & g_2 \\ f_{-1} & f_0 & f_1 & g_{-1} & g_0 & g_1 \end{array} \right) \\ &= \left(\begin{array}{ccc|cc} f_0 & f_1 & f_2 & g_0 & g_1 & g_2 \\ f_2 & f_0 & f_1 & g_2 & g_0 & g_1 \end{array} \right) \tag{4} \\ &= \left(\begin{array}{ccc|ccc} 5X + 7 & 5X + 3 & 1X + 6 & 5X + 7 & 5X + 5 & 5X + 7 \\ 1X + 6 & 5X + 7 & 5X + 3 & 5X + 7 & 5X + 7 & 5X + 5 \end{array} \right). \tag{5}\end{aligned}$$

The corresponding matrix \hat{H}_Z is defined analogously by replacing each block in \hat{H}_X with its inverse, arranged according to the shifted index pattern:

$$\begin{aligned}\hat{H}_Z &= \left(\begin{array}{ccc|cc} g_0^{-1} & g_{-1}^{-1} & g_{-2}^{-1} & f_0^{-1} & f_{-1}^{-1} & f_{-2}^{-1} \\ g_1^{-1} & g_0^{-1} & g_{-1}^{-1} & f_1^{-1} & f_0^{-1} & f_{-1}^{-1} \end{array} \right) \\ &= \left(\begin{array}{ccc|cc} g_0^{-1} & g_2^{-1} & g_1^{-1} & f_0^{-1} & f_2^{-1} & f_1^{-1} \\ g_1^{-1} & g_0^{-1} & g_2^{-1} & f_1^{-1} & f_0^{-1} & f_2^{-1} \end{array} \right) \\ &= \left(\begin{array}{ccc|ccc} 5X + 5 & 5X + 5 & 5X + 7 & 5X + 5 & 1X + 2 & 5X + 1 \\ 5X + 7 & 5X + 5 & 5X + 5 & 5X + 1 & 5X + 5 & 1X + 2 \end{array} \right).\end{aligned}$$

Let $M = JP = 16$ and $N = LP = 48$. The $M \times N$ binary matrices corresponding to \hat{H}_X and \hat{H}_Z are obtained by replacing each affine permutation with its associated $P \times P$ binary permutation matrix. The resulting binary matrices are shown below. The zero entries are represented as blanks. To facilitate understanding of the correspondence with the Tanner or factor graphs introduced in later sections, each block in the matrix is color-coded to match the corresponding edge in the graph. These matrices contain no cycles of length 4, but do contain cycles of length 8.

The binary matrices corresponding to $\hat{H}_X^{(2)}$ and $\hat{H}_Z^{(2)}$ are shown below. Each affine permutation is expanded into a $P \times P$ binary permutation matrix with $P = 8$.

$$\begin{aligned}
\hat{H}_Z^{(2)} &= \left(\begin{array}{ccc|cc} g_2^{-1} & g_1^{-1} & g_0^{-1} & f_2^{-1} & f_1^{-1} & f_0^{-1} \end{array} \right) \\
&= \left(\begin{array}{ccc|ccc} 5X+5 & 5X+7 & 5X+5 & 1X+2 & 5X+1 & 5X+5 \end{array} \right) \\
&= \left(\begin{array}{ccc|ccc|ccc|ccc|ccc} 1 & 1 & 1 & 1 & 1 & 1 & 1 & 1 & 1 & 1 & 1 & 1 & 1 \\ 1 & 1 & 1 & 1 & 1 & 1 & 1 & 1 & 1 & 1 & 1 & 1 & 1 \\ 1 & 1 & 1 & 1 & 1 & 1 & 1 & 1 & 1 & 1 & 1 & 1 & 1 \\ 1 & 1 & 1 & 1 & 1 & 1 & 1 & 1 & 1 & 1 & 1 & 1 & 1 \\ 1 & \textcolor{red}{1} \\ 1 & 1 & 1 & 1 & 1 & 1 & 1 & 1 & 1 & 1 & 1 & 1 & 1 \end{array} \right).
\end{aligned}$$

□

This construction generalizes the original Hagiwara–Imai construction [13], [30] to a more flexible framework involving general PMs [31], by extending the class of permutations from \mathcal{Q}_P to \mathcal{F}_P . Under the condition specified in Requirement 1, the matrices $\hat{H}_X, \hat{H}_Z \in \mathbb{F}_2^{JP \times LP}$ are orthogonal, i.e.,

$$\hat{H}_X \hat{H}_Z^\top = O. \quad (6)$$

This orthogonality follows from the structure of the circulant blocks. Specifically, the (j, k) -th block of the product is given by

$$\begin{aligned}
(\hat{H}_X \hat{H}_Z^\top)_{j,k} &= \sum_{\ell} F_{\ell-j} G_{k-\ell} + \sum_{\ell} G_{\ell-j} F_{k-\ell} \\
&= \sum_{\ell} F_{\ell-j} G_{k-\ell} + \sum_{\ell} F_{k-\ell} G_{\ell-j} \\
&= \sum_{\ell} F_{\ell} G_{k-j-\ell} + \sum_{\ell} F_{-\ell} G_{\ell-j+k} \\
&= \sum_{\ell} F_{\ell} G_{k-j-\ell} + \sum_{\ell} F_{\ell} G_{k-j-\ell} \\
&= O,
\end{aligned}$$

In all summations above, the index ℓ ranges over $[L/2]$. The first equality follows from Requirement 1, and the final equality holds since the two sums are identical over \mathbb{F}_2 and thus cancel out. Therefore, \hat{H}_X and \hat{H}_Z are orthogonal by construction.

III-B Construction of Non-binary Parity-Check Matrices H_Γ and H_Δ

In the previous section, we constructed a pair of orthogonal (J, L) -regular binary LDPC matrices, \hat{H}_X and \hat{H}_Z . Let $q = 2^e$ for a positive integer e . In this section, we focus on the case $J = 2$ and outline the conventional method [31], which generalizes the earlier approach by Kasai et al. [30] for constructing a pair of orthogonal LDPC matrices H_Γ and H_Δ over \mathbb{F}_q . These matrices share the same support as \hat{H}_X and \hat{H}_Z , and serve as the basis for the modified construction in Section V.

We consider $H_\Gamma, H_\Delta \in \mathbb{F}_q^{J \times L}$ with the same support as \hat{H}_X and \hat{H}_Z . Our goal is to randomly generate such matrices satisfying the orthogonality condition

$$H_\Gamma H_\Delta^\top = O. \quad (7)$$

When $J \geq 3$, this condition leads to a system of quadratic equations over \mathbb{F}_q , which is generally intractable. However, for $J = 2$, the problem can be decomposed into two linear subproblems, allowing for efficient solution via linear algebra.

We denote the entries of the matrices as follows:

$$H_\Gamma = (\gamma_{ij}), \quad H_\Delta = (\delta_{ij}).$$

To express the algorithm concisely, we define a one-dimensional vector representation in place of (γ_{ij}) and (δ_{ij}) . Let us define a vector representation $\underline{\gamma} = (\gamma_0, \dots, \gamma_{2N-1}) \in \mathbb{F}_q^{2N}$ associated with the parity-check matrix H_Γ as follows. For each position (i, j) such that $(\hat{H}_X)_{ij} \neq 0$, we define:

$$\gamma_{i,j} = \begin{cases} \gamma_j & \text{if } i < P, \\ \gamma_{j+PL} & \text{if } i \geq P. \end{cases}$$

Since H_Γ contains exactly $2N$ nonzero entries, the length of the vector $\underline{\gamma}$ is also $2N$. The corresponding vector $\underline{\delta}$ associated with H_Δ is defined analogously.

Each nonzero entry such as 0F represents the field element α^{15} , where α is a fixed primitive element of \mathbb{F}_q , and the exponent is the decimal equivalent of the hexadecimal value. The nonzero support (positions) of H_Γ and H_Δ matches those of the corresponding binary matrices \hat{H}_X and \hat{H}_Z . The matrices H_Γ and H_Δ are constructed to be orthogonal. For example, let us examine the orthogonality between the 7th row of H_Γ and the 5th row of H_Δ . These rows contain the following intersecting non-zero entries:

$$H_\Gamma[7, \cdot] = (\alpha^{200}, \alpha^{238}), \quad H_\Delta[5, \cdot] = (\alpha^{62}, \alpha^{24}).$$

Then, their inner product is given by:

$$\alpha^{200} \cdot \alpha^{62} + \alpha^{238} \cdot \alpha^{24} = \alpha^{(200+62) \bmod 255} + \alpha^{(238+24) \bmod 255} = \alpha^7 + \alpha^7 = 0.$$

This confirms that the two rows are orthogonal over \mathbb{F}_{256} .

III-C Construction of H_X and H_Z

In this section, we construct orthogonal \mathbb{F}_2 -valued matrices H_X and H_Z of size $m \times n$ from the orthogonal \mathbb{F}_q -valued matrices H_Γ and H_Δ of size $M \times N$ obtained in the previous section, where $n = eN$ and $m = eM$. This construction follows the method used in [30] and [31]. The matrices H_X and H_Z are constructed from H_Γ and H_Δ as follows. The theoretical justification and proofs, which were omitted in [30] and [31], are provided in the appendices.

The companion matrix $A(\gamma) \in \mathbb{F}_2^{n \times n}$ for $\gamma \in \mathbb{F}_q$ are defined in Appendices A. Using the mapping A , we construct the binary parity-check matrices (H_X, H_Z) as follows:

$$H_X = (A(\gamma_{i,j})), \quad H_Z = (A(\delta_{i,j})^\top).$$

From the properties of the companion matrix, it can be verified that (H_X, H_Z) are orthogonal:

$$H_X H_Z^\dagger = O. \quad (11)$$

A proof of (11) is provided in Appendix C.

We denote by C_Γ and C_Δ the \mathbb{F}_q -linear spaces defined as the null spaces of the matrices H_Γ and H_Δ , respectively:

$$C_\Gamma = \{\underline{\xi} \in \mathbb{F}_q^N \mid H_\Gamma \underline{\xi} = 0\}, \quad C_\Delta = \{\underline{\xi} \in \mathbb{F}_q^N \mid H_\Delta \underline{\xi} = 0\}.$$

Likewise, we denote by C_X and C_Z the \mathbb{F}_2 -linear spaces defined as the null spaces of the binary matrices H_X and H_Z , respectively:

$$C_X = \{\underline{x} \in \mathbb{F}_2^n \mid H_X \underline{x} = 0\}, \quad C_Z = \{\underline{x} \in \mathbb{F}_2^n \mid H_Z \underline{x} = 0\}.$$

The following theorem shows that the codes C_Γ and C_Δ , originally defined over \mathbb{F}_q , can be equivalently represented as binary codes C_X and C_Z via the transformations \underline{v} and \underline{w} , respectively. The definitions of the mappings $\underline{v}(\cdot)$ and $\underline{w}(\cdot)$ are provided in Appendices A and B.

Theorem 2. Let $\xi = (\xi_0, \dots, \xi_{N-1})$ be a vector over \mathbb{F}_q . Then the following statements hold:

- 1) $(\underline{v}(\xi_0), \dots, \underline{v}(\xi_{N-1})) \in C_X$ if and only if $\underline{\xi} \in C_\Gamma$.
 - 2) $(\underline{w}(\xi_0), \dots, \underline{w}(\xi_{N-1})) \in C_Z$ if and only if $\underline{\xi} \in C_\Delta$.

Proof. From Appendix A and Appendix B, we obtain the following identities for any vector $\xi = (\xi_0, \dots, \xi_{N-1}) \in \mathbb{F}_q^N$:

$$\sum_j (H_X)_{ij} \underline{v}(\xi_j) = \sum_j A(\gamma_{ij}) \underline{v}(\xi_j) = \sum_j \underline{v}(\gamma_{ij} \xi_j) = \underline{v} \left(\sum_j \gamma_{ij} \xi_j \right),$$

$$\sum_j (H_Z)_{ij} \underline{w}(\xi_j) = \sum_j A(\delta_{ij})^\top \underline{w}(\xi_j) = \sum_j \underline{w}(\delta_{ij} \xi_j) = \underline{w} \left(\sum_j \delta_{ij} \xi_j \right).$$

These equalities show that applying H_X to the bit-level expansion $(\underline{v}(\xi_0), \dots, \underline{v}(\xi_{N-1}))$ is equivalent to applying H_Γ to ξ over \mathbb{F}_q and then mapping the result via \underline{v} . Therefore, $(\underline{v}(\xi_0), \dots, \underline{v}(\xi_{N-1}))$ belongs to C_X if and only if $\xi \in C_\Gamma$. The second statement is proved in the same way. \square

This correspondence allows us to identify (C_X, C_Z) with (C_Γ, C_Δ) . For example, we write

$$C_X = C_\Gamma, \quad C_Z = C_\Delta.$$

In particular, the orthogonality condition $C_X^\perp \subset C_Z$ is equivalent to $C_\Gamma^\perp \subset C_\Delta$.

The binary CSS code defined by (C_X, C_Z) is used for quantum error correction. As explained in Section VI, the decoder does not directly use the binary matrices H_X and H_Z as the binary matrices that define the Tanner graphs for BP decoding. Instead, it uses a partitioned form of H_X and H_Z divided into e -bit blocks, or equivalently, the corresponding nonbinary matrices H_Γ and H_Δ . Accordingly, when we refer to the girth of C_X or C_Z , we mean the girth of H_Γ or H_Δ , respectively; that is, the girth of \hat{H}_X or \hat{H}_Z .

The minimum distance d is defined as follows, where $w_H(\cdot)$ denotes the Hamming weight of a binary vector:

$$\begin{aligned} d_X &= \min_{\underline{x} \in C_X \setminus C_Z^\perp} w_H(\underline{x}) \\ &= \min_{\underline{\xi} \in C_\Gamma \setminus C_\Delta^\perp} w_H(\underline{v}(\xi_0), \underline{v}(\xi_1), \dots, \underline{v}(\xi_{N-1})), \end{aligned} \tag{12}$$

$$\begin{aligned} d_Z &= \min_{\underline{z} \in C_Z \setminus C_X^\perp} w_H(\underline{z}) \\ &= \min_{\underline{\zeta} \in C_\Delta \setminus C_\Gamma^\perp} w_H(\underline{w}(\zeta_0), \underline{w}(\zeta_1), \dots, \underline{w}(\zeta_{N-1})), \\ d &= \min\{d_X, d_Z\}. \end{aligned} \tag{13}$$

IV Structure of Cycles in the Conventional Method

From this section onward, we assume a fixed row weight L , unless stated otherwise. To emphasize the structural role of L in the design and analysis of the code, we avoid substituting expressions involving L (such as $2L$ or $L/2$) with their explicit numeric values (e.g., $2L = 12$, $L/2 = 3$). Instead, we consistently retain symbolic expressions in terms of L throughout the presentation.

In this section, we investigate properties of the Tanner graphs associated with the parity-check matrices of CSS codes constructed using the conventional method. In Section IV-A, we show that the matrices H_X and H_Z (or equivalently \hat{H}_X and \hat{H}_Z) inevitably contain three types of TCBCs of length $2L$, denoted by $\underline{u}(j)$ for $j = \{0, 1, 2\}$. Next, in Section IV-B, we demonstrate that the structures of $\underline{u}(j)$ for $j = \{0, 1\}$ in H_X and H_Z correspond to codewords in C_Z^\perp and C_X^\perp , respectively. Furthermore, we show that the structure of $\underline{u}(2)$ in H_X and H_Z corresponds to codewords in $C_X \setminus C_Z^\perp$ and $C_Z \setminus C_X^\perp$, respectively.

IV-A Unavoidable Totally Closed Block Cycles

Suppose that \hat{H}_X and \hat{H}_Z are constructed from f and g according to the method described in Definition 1. The following theorem states that, under Requirement 1, the existence of length- $2L$ TCBCs is inevitable in the construction of the parity-check matrices \hat{H}_X and \hat{H}_Z .

Theorem 3 (Unavoidable TCBCs [31]). Let $P \geq 1$. Let f and g be permutations in \mathcal{F}_P that satisfy Requirement 1. For each integer $j \in \{0, 1, 2\}$, consider a following block cycle $\underline{u}(j)$ of length $2L$ in \hat{H}_X , starting from position $(0, 0)$:

$$\underline{u}(j) = f_0 \Rightarrow g_j \Rightarrow f_1 \Rightarrow g_{j-1} \Rightarrow \dots \Rightarrow f_{L/2-1} \Rightarrow g_{j-(L/2-1)} \Rightarrow f_0. \tag{14}$$

Each block cycle $\underline{u}(j)$ forms a TCBC in \hat{H}_X . Note that the subscripts of f and g are to be interpreted modulo $L/2$, i.e., as elements of $\mathbb{Z}_{L/2}$.

A symmetric statement holds for a block cycle in \hat{H}_Z , which is obtained by interchanging the roles of X and Z . The corresponding block cycle is given by:

$$\underline{u}(j) = g_0^{-1} \Rightarrow f_{-j}^{-1} \Rightarrow g_{-1}^{-1} \Rightarrow f_{-(j-1)}^{-1} \Rightarrow \dots \Rightarrow g_{-(L/2-1)}^{-1} \Rightarrow f_{-(j-(L/2-1))}^{-1} \Rightarrow g_0^{-1}. \tag{15}$$

Each block cycle $\underline{u}(j)$ forms a TCBC in \hat{H}_Z .

Proof. Let $f_{\underline{u}(j)}$ denote the composed function corresponding to $\underline{u}(j)$ in (14). The simplified block cycle in (14) can be expanded into the full block cycle form as follows:

$$\underline{u}(j) = f_0 \rightarrow g_j \rightarrow g_{j-1} \rightarrow f_0 \rightarrow f_1 \rightarrow g_{j-1} \rightarrow g_{j-2} \rightarrow f_1 \rightarrow \dots \rightarrow f_{L/2-1} \rightarrow g_{j-L/2-1} \rightarrow g_{j-(L/2)} \rightarrow f_{L/2-1} \rightarrow f_0$$

Therefore, the composite function of $\underline{u}(j)$ is calculate

$$\begin{aligned}
f_{\underline{u}(j)}^{-1} &= (f_0^{-1} g_j g_{j-1}^{-1} f_0)(f_1^{-1} g_{j-1} g_{j-2}^{-1} f_1) \cdots (f_\ell^{-1} g_{j-\ell} g_{j-(\ell+1)}^{-1} f_\ell) \cdots (f_{L/2-1}^{-1} g_{j-L/2-1} g_{j-(L/2)}^{-1} f_{L/2-1}) \\
&= (g_j g_{j-1}^{-1} f_0 f_0^{-1})(g_{j-1} g_{j-2}^{-1} f_1 f_1^{-1}) \cdots (g_{j-\ell} g_{j-(\ell+1)}^{-1} f_\ell f_\ell^{-1}) \cdots (g_{j-L/2-1} g_{j-(L/2)}^{-1} f_{L/2-1} f_{L/2-1}^{-1}) \\
&= (g_j g_{j-1}^{-1})(g_{j-1} g_{j-2}^{-1}) \cdots (g_{j-\ell} g_{j-(\ell+1)}^{-1}) \cdots (g_{j-L/2-1} g_{j-(L/2)}^{-1}) \\
&= g_j(g_{j-1}^{-1} g_{j-1})(g_{j-2}^{-1} g_{j-2}) \cdots (g_{j-\ell}^{-1} g_{j-\ell}) \cdots (g_{j-L/2-1}^{-1} g_{j-L/2-1}) g_{j-(L/2)}^{-1} \\
&= g_j g_{j-(L/2)}^{-1} \\
&= g_j g_j^{-1} \\
&= \text{id}.
\end{aligned}$$

Here, we used Lemma 1 and condition (3), which is equivalent to Requirement 1. Under this condition, the following identities hold.

$$\begin{aligned}
f_\ell^{-1} g_{j-\ell} &= g_{j-\ell} f_\ell^{-1}, \\
f_\ell g_{j-(\ell+1)}^{-1} &= g_{j-(\ell+1)}^{-1} f_\ell,
\end{aligned}$$

for $\ell \in [L/2]$. In particular, f_ℓ and $g_{\ell'}$ commute for all $\ell, \ell' \in [L/2]$ when $L = 6$. In the same manner, it can be shown that the composition of the functions along the block cycle in (15) also yields the identity function. \square

In [31], the target codes had $L \geq 8$, and Theorem 3 was applied only for $j = 0, 1$. In contrast, the present paper focuses on the case $L = 6$, for which the theorem also holds for $j = 2$. The newly identified TCBC $\underline{u}(2)$ was found to be a dominant source of performance degradation specifically when $L = 6$. In this work, we propose non-binary label assignment scheme that neutralizes the harmful effect of $\underline{u}(2)$, thereby enabling improved decoding performance.

Thus, while Theorem 3 guarantees the existence of TCBCs denoted by $\underline{u}(j)$, it leaves open the possibility that other types of TCBC may exist. However, Example 3, together with Table II, provides an explicit instance of $\underline{f}, \underline{g}$ in which no closed block cycles other than $\underline{u}(j)$ appear for any $P \geq 1$. This observation suggests that $\underline{u}(j)$ identified in Theorem 3 are the only ones that necessarily occur.

We refer to these as *unavoidable TCBCs* (UTCBCs), denoted by (14) and (15) in \hat{H}_X and \hat{H}_Z , respectively. When the context is clear, we simply denote them by $\underline{u}(j)$. Depending on the context, the UTCBC $\underline{u}(j)$ in \hat{H}_X may be regarded as the set of Tanner cycles contained within it. Moreover, when we refer to the UTCBC $\underline{u}(j)$ in H_Γ , we mean the submatrix in H_Γ corresponding to the Tanner cycles that comprise $\underline{u}(j)$ in \hat{H}_X , including their non-binary matrix components. Likewise, the UTCBC $\underline{u}(j)$ in H_X refers to the corresponding submatrix in H_X that aligns with the UTCBC $\underline{u}(j)$ in H_Γ .

Example 5. In the matrices \hat{H}_X and \hat{H}_Z provided in Example 3, two Tanner cycles contained in each $\underline{u}(j)$ for $j = 2$ and $j = 0$ is highlighted in red and blue, respectively. In the matrices H_Γ and H_Δ provided in Example 4, two Tanner cycles contained in each $\underline{u}(j)$ for $j = 2$ and $j = 0$ is highlighted in red and blue, respectively.

We consider the parity-check matrices \hat{H}_X and \hat{H}_Z with block dimensions $J = 2$ and $L = 6$. Each matrix comprises $J \times L$ blocks, where each block is of size $P \times P$. Under this configuration, each $\underline{u}(j)$ traverses all blocks exactly once. For $j \in \{0, 1, 2\}$, we illustrate the sequence in which the blocks are visited in $\underline{u}(j)$, starting from position $(0, 0)$. The blocks are labeled in the order $0, 1, 2, \dots, 10, 11$. The following matrices represent the visitation order over the 2×6 grid of blocks:

$$\left(\begin{array}{ccccc|cc} 0 & 4 & 8 & 1 & 9 & 5 \\ 11 & 3 & 7 & 2 & 10 & 6 \end{array} \right), \quad \left(\begin{array}{ccccc|cc} 0 & 4 & 8 & 5 & 1 & 9 \\ 11 & 3 & 7 & 6 & 2 & 10 \end{array} \right), \quad \left(\begin{array}{ccccc|cc} 0 & 4 & 8 & 9 & 5 & 1 \\ 11 & 3 & 7 & 10 & 6 & 2 \end{array} \right)$$

Each matrix corresponds to $j = 0$, $j = 1$, and $j = 2$, respectively. It can be verified that each of these block cycles $\underline{u}(j)$ visits all $J \times L$ blocks exactly once by circulating $L/2$ steps clockwise through the four quadrants of the matrix, each consisting of half rows or half columns. This structure ensures that the entire matrix is covered uniformly in a single traversal. \square

Theorem 4 concerns the structure of the UTCBCs $\underline{u}(k)$ for $k \in \{0, 1, 2\}$ in \hat{H}_X and \hat{H}_Z . Before stating the theorem, we first present the following illustrative example. Let h_{kr}^\top denote the r -th row of $\hat{H}_X^{(k)}$. From the orthogonality condition (6), this row is expected to be orthogonal to \hat{H}_Z , satisfying the following relation:

$$\hat{H}_Z h_{kr} = \underline{0}.$$

Let us recall the matrices \hat{H}_X and \hat{H}_Z discussed in Example 3. For the case $k = 0$ and $r = 7$, the nonzero entries involved in the equation are located at columns 0, 12, 17, 24, 34, and 40, and at rows 1, 4, 5, 9, 10, and 15. These entries are extracted and presented as follows:

$$\begin{pmatrix} 1 & & & & 1 \\ & 1 & & 1 & \\ & & 1 & 1 & \\ 1 & & & 1 & \\ & 1 & & 1 & \\ & & 1 & 1 & \\ & & & 1 & \end{pmatrix} \begin{pmatrix} 1 \\ 1 \\ 1 \\ 1 \\ 1 \\ 1 \end{pmatrix} = 0$$

The submatrix of \hat{H}_Z that appears in the above equation is an $L \times L$ matrix forming a Tanner cycle of length $2L$. We refer to this submatrix as S . Moreover, it can be verified that S is contained in the UTCBC $\underline{u}(0)$ in \hat{H}_Z . Theorem 4 asserts that this property holds for any $j \in [J]$ and $r \in [P]$, under Requirement 1 together with Requirement 2.

Requirement 2 is a condition imposed specifically on the permutation pair $(\underline{f}, \underline{g})$ to ensure that the submatrix S is square. To describe the condition that guarantees injectivity within the indexing structure of S , we define a set of composed functions as follows:

$$\mathcal{F} := \{f_{\ell-k} \circ g_{-(\ell-j)} \mid \ell \in [L/2], j \in [J], k \in \{0, 1, 2\}\}.$$

Requirement 2. Let us say that two functions $f, g \in \mathcal{F}_P$ intersect if there exists $j \in \mathbb{Z}_P$ such that $f(j) = g(j)$. We require that every pair of distinct functions $h, h' \in \mathcal{F}$ do not intersect; that is,

$$h(j) \neq h'(j) \quad \text{for all } j \in [P].$$

□

As discussed in the proof of the following theorem, if Requirement 2 is not satisfied, then cycles of length less than $2L$ will appear in \hat{H}_X and \hat{H}_Z . If the permutations \underline{f} and \underline{g} are constructed so that the girth is exactly $2L$, then Requirement 2 is automatically satisfied. When L is small—particularly in the case $L = 6$, which is the main focus of this paper—the girth is explicitly set to $2L$. Therefore, it is not necessary to explicitly impose Requirement 2 in the code design process.

In the following, we restrict our attention to those permutations $(\underline{f}, \underline{g})$ and the corresponding parity-check matrices (\hat{H}_X, \hat{H}_Z) that satisfy both Requirement 1 and Requirement 2.

Theorem 4 (Properties of the UTCBCs). For any $k \in \{0, 1, 2\}$, let the r -th row of the block $\hat{H}_X^{(k)}$ be denoted by \underline{h}_{kr}^\top , where $r \in [P]$. Here, \underline{h}_{kr} is a binary vector of length $N = LP$. Then, by the orthogonality condition (6), the following must hold:

$$\hat{H}_Z \underline{h}_{kr} = \underline{0}.$$

Let S denote the submatrix of \hat{H}_Z involved in this equation, corresponding to the nonzero positions of \underline{h}_{kr} . Then, the submatrix S is square, forms a Tanner cycle of length $2L$, and moreover, it belongs to the UTCBC $\underline{u}(k)$ in \hat{H}_Z , as defined in Theorem 3. The same conclusion holds when the roles of \hat{H}_Z and \hat{H}_X are interchanged.

Proof. While the proof is not particularly difficult, it is unfortunately not easy to present in a concise form. Therefore, we recommend the reader to refer to Example 6, which illustrates concrete instances of the key expressions used in the proof.

For $j \in [J]$ and $r \in [P]$, we denote the r -th row within the j -th row block by $[r, j]$, which corresponds to the absolute row index $jP + r$ in the matrix \hat{H}_X or \hat{H}_Z . For column indices, we use the column block index $\ell \in [L/2]$ to refer to columns within the left and right halves of \hat{H}_X or \hat{H}_Z , which each consist of $L/2$ blocks. For $c \in [P]$, the c -th column within the ℓ -th column block of the left half is denoted by $[c, \ell]_L$, which corresponds to the absolute column index $\ell P + c$. The c -th column within the ℓ -th column block of the right half is also denoted by $[c, \ell]_R$, but corresponds to the absolute column index $(\ell + L/2)P + c$.

We begin by analyzing the columns of the submatrix S ; that is, we examine the column indices corresponding to the nonzero entries of \underline{h}_{kr} . Recall that \underline{h}_{kr} is the r -th row of the matrix $\hat{H}_X^{(k)}$. In $\hat{H}_X^{(k)}$, the ℓ -th column block in the left and right halves corresponds to the permutations $f_{\ell-k}$ and $g_{\ell-k}$, respectively. In each half, each column $c \in [P]$ contains a 1 at position $([f_{\ell-k}(c), k], [c, \ell]_L)$ in the left half and $([g_{\ell-k}(c), k], [c, \ell]_R)$ in the right half. Equivalently, in the left and right halves, respectively, for each row index $r \in [P]$, the entries at positions $([r, k], [f_{\ell-k}^{-1}(r), \ell]_L)$ and $([r, k], [g_{\ell-k}^{-1}(r), \ell]_R)$ are equal to 1. By extending this idea to the right half as well, we now describe the positions of 1's in the binary vector \underline{h}_{kr} . It can be seen that one column of S appears in each column block among the L column blocks of $\hat{H}_Z^{(k)}$. That is, S has one column in each of the L blocks.

$$c_{L,0} \mid c_{L,1} \mid \cdots \mid c_{L,L/2-1} \parallel c_{R,0} \mid c_{R,1} \mid \cdots \mid c_{R,L/2-1} \tag{16}$$

Here, the column indices are defined as:

$$c_{L,\ell} = f_{\ell-k}^{-1}(r), \quad c_{R,\ell} = g_{\ell-k}^{-1}(r).$$

Each $c_{L,\ell}$ (respectively $c_{R,\ell}$) corresponds to the index of the column within the ℓ -th column block of the left (respectively right) half of $\hat{H}_Z^{(k)}$ that contains a 1 in the r -th row.

Next, we analyze the rows of the submatrix S . In the (j, ℓ) -th block of the left half of \hat{H}_Z for $j \in [J]$ and $\ell \in [L/2]$, which corresponds to the permutation $g_{-(\ell-j)}^{-1}$, the entry at position $(g_{-(\ell-j)}^{-1}(c_{L,0}), c_{L,0})$ is equal to 1. Proceeding similarly, the entries in $\hat{H}_X^{(0)}$ and $\hat{H}_X^{(1)}$ that intersect with the support of \underline{h}_{kr} are located at the following positions:

$$\begin{array}{c|c} (r_{0,\ell}, c_{L,\ell})_{\ell=0,1,\dots,L/2-1} & (s_{0,\ell}, c_{R,\ell})_{\ell=0,1,\dots,L/2-1} \\ \hline (r_{1,\ell}, c_{L,\ell})_{\ell=0,1,\dots,L/2-1} & (s_{1,\ell}, c_{R,\ell})_{\ell=0,1,\dots,L/2-1} \end{array} \quad (17)$$

where the row indices are defined as

$$r_{j,\ell} = g_{-(\ell-j)}^{-1}(c_{L,\ell}) = (g_{-(\ell-j)}^{-1}f_{\ell-k}^{-1})(r), \quad s_{j,\ell} = f_{-(\ell-j)}^{-1}(c_{R,\ell}) = (f_{-(\ell-j)}^{-1}g_{\ell-k}^{-1})(r).$$

By the commutativity condition (2), which is equivalent to Requirement 1, namely $f_{\ell-j}g_{k-\ell} = g_{k-\ell}f_{\ell-j}$ for all $\ell \in [L/2]$, $j, k \in [J]$, and by applying Lemma 1, the left and right row indices in (17) are equal as sets. More precisely, we have

$$\{r_{j,0}, r_{j,1}, \dots, r_{j,L/2-1}\} = \{s_{j,0}, s_{j,1}, \dots, s_{j,L/2-1}\} \quad \text{for all } j \in [J],$$

with the correspondence given explicitly by

$$r_{j,\ell} = s_{j,j+k-\ell}, \quad r_{j,j+k-\ell} = s_{j,\ell}.$$

Furthermore, by Requirement 2, each of these sets consists of $L/2$ distinct row indices. Consequently, the submatrix S is an $L \times L$ square matrix in which every row and every column has weight two. It remains to show that this matrix forms a cycle of length $2L$. Conversely, if Requirement 2 is not satisfied, then the number of rows in S becomes smaller than L , and a cycle of length less than $2L$ will appear within S .

We now describe a specific closed cycle in S , which is part of a block cycle winding around the four quadrants of \hat{H}_X . This cycle traverses the four regions into which \hat{H}_X is divided by its horizontal and vertical halves, proceeding clockwise through them over $L/2$ steps. Consider the entry

$$([r_{0,0}, 0], [c_{L,0}, 0]_L)$$

in block $(0,0)$, located in the upper-left quadrant. This is the starting point of the Tanner cycle. During the ℓ -th round ($\ell = 0, 1, \dots, L/2 - 1$), the traversal proceeds as follows:

Start:	$([r_{0,\ell}, 0], [c_{L,\ell}, \ell]_L)$
Right move:	$([r_{0,\ell} = s_{0,k-\ell}, 0], [c_{R,k-\ell}, k-\ell]_R)$
Down move:	$([s_{1,k-\ell}, 1], [c_{R,k-\ell}, k-\ell]_R)$
Left move:	$([r_{1,\ell+1} = s_{1,k}, 1], [c_{L,\ell+1}, \ell+1]_L)$
Up move:	$([r_{0,\ell+1}, 0], [c_{L,\ell+1}, \ell+1]_L)$

By viewing \hat{H}_X as consisting of four quadrants (upper-left, upper-right, lower-right, and lower-left), we see that the block cycle rotates clockwise, completing $L/2$ full rounds. The sets of column indices in the left and right halves of \hat{H}_X are given by

$$C_L = ([c_{L,\ell}, \ell]_L)_{\ell=0,1,\dots,L/2-1}, \quad C_R = ([c_{R,\ell}, \ell]_R)_{\ell=0,1,\dots,L/2-1}.$$

The sets of row indices in the upper and lower halves of \hat{H}_Z are defined as

$$R_0 = ([r_{0,\ell} 0])_{\ell=0,1,\dots,L/2-1},$$

$$R_1 = ([r_{1,\ell} 1])_{\ell=0,1,\dots,L/2-1}.$$

The corresponding submatrix of \hat{H}_X that connects these row and column sets, with entries corresponding to 1s, can be compactly represented as follows:

$$\begin{array}{c|c|c} & C_L & C_R \\ \hline \hline R_0 & I & M^{(k)} \\ \hline R_1 & I & M^{(k+1)} \end{array} \quad (18)$$

Here, I denotes the identity matrix of size $L \times L$, and $M^{(k)}$ denotes a permutation matrix of size $L/2 \times L/2$ defined by

$$M_{ij}^{(k)} = \begin{cases} 1 & \text{if } i + j \equiv k \pmod{L/2}, \\ 0 & \text{otherwise.} \end{cases}$$

The Tanner cycle in question is contained in a block cycle, which can be expressed in a simplified form for $J = 2$ as follows:

$$\underline{u}(j) = g_0^{-1} \Rightarrow f_{-j}^{-1} \Rightarrow g_{-1}^{-1} \Rightarrow f_{-(j-1)}^{-1} \Rightarrow \cdots \Rightarrow g_{-(L/2-1)}^{-1} \Rightarrow f_{-(j-(L/2-1))}^{-1} \Rightarrow g_0^{-1}.$$

This sequence coincides with the UTCBC $\underline{u}(k)$ in \hat{H}_Z , as defined in (15) of Theorem 3. A similar argument applies to the case obtained by interchanging X and Z . \square

Example 6. Let us recall the example discussed in Example 3. For $k = 0$ and $r = 7$, we consider the submatrix S involved in the equation

$$\hat{H}_Z \underline{h}_{kr} = \underline{0},$$

where \underline{h}_{kr}^\top is the r -th row of $\hat{H}_X^{(k)}$. The sets in (16) are instantiated as follows:

$c_{L,0}$	$c_{L,1}$	$c_{L,2}$	$c_{R,0}$	$c_{R,1}$	$c_{R,2}$
0	4	1	0	2	0

The positions in (17) are given explicitly as:

$(r_{0,0}, c_{L,0})$	$(r_{0,1}, c_{L,1})$	$(r_{0,2}, c_{L,2})$	$(s_{0,0}, c_{R,0})$	$(s_{0,1}, c_{R,1})$	$(s_{0,2}, c_{R,2})$
(5, 0)	(1, 4)	(4, 1)	(5, 0)	(4, 2)	(1, 0)
(7, 0)	(1, 4)	(2, 1)	(1, 0)	(7, 2)	(2, 0)

The submatrix representation in (18) is instantiated as:

	$[0, 0]_L$	$[4, 1]_L$	$[1, 2]_L$	$[0, 0]_R$	$[2, 1]_R$	$[0, 2]_R$
[5, 0]	1			1		
[1, 0]		1				1
[4, 0]			1		1	
[7, 1]	1				1	
[1, 1]		1			1	
[2, 1]			1			1

\square

IV-B Impact of UTCBCs on Minimum Distance

Following common conventions in the literature on LDPC codes, we identify the Tanner graph G corresponding to the matrix H_Γ with H_Γ itself. Accordingly, columns correspond to variable nodes, rows to check nodes, and submatrices to subgraphs, allowing us to treat these elements interchangeably. For example, the Tanner graph associated with a submatrix S of H_Γ is also denoted by S . Similarly, a subgraph of H_Γ is denoted by G' , and the corresponding submatrix is also referred to as G' .

Let us consider a Tanner cycle C of length $2L$ contained in H_Γ . Let $(H_\Gamma)_C$ denote the submatrix of H_Γ obtained by zeroing out all columns not involved in the cycle C . Similarly, let $\underline{\xi}_C$ denote the vector obtained from $\underline{\xi} \in \mathbb{F}_q^N$ by zeroing out all coordinates not corresponding to columns in C . We define the subcode associated with the cycle C as

$$N(C; H_\Gamma) \stackrel{\text{def}}{=} \left\{ \underline{\xi}_C \in \mathbb{F}_q^N \mid (H_\Gamma)_C \underline{\xi}_C = \underline{0}, \underline{\xi} \in \mathbb{F}_q^N \right\}.$$

The set $N(C; H_\Gamma)$ is a subcode of C_Γ , supported only on the positions involved in the cycle C . It captures the contribution of the cycle C to the code C_Γ by isolating codewords whose nonzero positions lie solely within C . Theorem 5 shows that $N(C; H_\Gamma)$ is contained in $C_\Delta^\perp \subset C_\Gamma$, and therefore such codewords do not affect the minimum distance d_X (see (12)).

Theorem 5. Let C be a Tanner cycle in the UTCBC $\underline{u}(k)$ in H_Γ for $k = 0, 1$, which is orthogonal to the row vector \underline{h}_{kr}^\top , in the sense that

$$(H_\Gamma)_C \underline{h}_{kr} = \underline{0}. \quad (19)$$

Here, \underline{h}_{kr}^\top denotes the r -th row of $H_\Delta^{(k)}$. Then, the associated subcode $N(\mathbf{C}; H_\Gamma)$ is a one-dimensional subspace over \mathbb{F}_q given by

$$N(\mathbf{C}; H_\Gamma) = \{\xi \underline{h}_{kr} \mid \xi \in \mathbb{F}_q\}, \quad (20)$$

where ξ is a scalar in \mathbb{F}_q . Moreover, $N(\mathbf{C}; H_\Gamma)$ is a subspace of $C_\Delta^\perp \subset C_\Gamma$. A similar statement holds when H_Δ is considered in place of H_Γ , i.e., when the roles of X and Z are interchanged.

Proof. We first observe that $\text{supp}(\underline{h}_{kr}) = \text{supp}(\mathbf{C})$. By Theorem 4, the cycle \mathbf{C} is square-shaped and can be arranged into an upper-triangular form except for one row. Therefore, its rank is at least $L - 1$. Since the column weight is $J = 2$, the rank of the submatrix $(H_\Gamma)_\mathbf{C}$ coincides with that of the cycle \mathbf{C} . From (19), a nonzero solution \underline{h}_{kr} exists in the kernel of $(H_\Gamma)_\mathbf{C}$, implying that its rank is at most $L - 1$. Hence, the rank of $(H_\Gamma)_\mathbf{C}$ is exactly $L - 1$, and this proves (20). Since \underline{h}_{kr}^\top is a row of the parity-check matrix H_Δ , it follows that $N(\mathbf{C}; H_\Gamma)$ is a subspace of C_Δ^\perp . \square

Example 7. As an example, consider the cycle \mathbf{C} in H_Δ highlighted in blue in Example 4. Consequently, $N(\mathbf{C}; H_\Gamma)$ is a subspace of C_Δ^\perp . Here, \underline{h}_{kr}^\top is the r -th row of $H_\Gamma^{(k)}$ for $k = 0, r = 7$, which is also highlighted in blue:

$$\underline{h}_{kr}^\top = (\alpha^{200} 0 0 0 0 0 0 0 0 0 \alpha^{200} 0 0 0 0 \alpha^{170} 0 0 0 0 0 0 \alpha^{238} 0 0 0 0 0 0 0 0 \alpha^{167} 0 0 0 0 0 \alpha^{95} 0 0 0 0 0 0 0).$$

We extract only the nonzero components involved in the equation $H_\Delta \underline{h}_{kr}^\top = \underline{0}$. The relevant portion can be represented as the following matrix-vector product:

$$\begin{pmatrix} & \text{7C} & & & \text{E5} \\ & 12 & 15 & & \\ \text{3E} & & & & \\ & 1D & 18 & & \\ & & F6 & & \\ & C2 & & & \text{OE} \\ \text{6F} & & & 90 & \end{pmatrix} \begin{pmatrix} \text{C8} \\ \text{C8} \\ \text{AA} \\ \text{EE} \\ \text{A7} \\ \text{5F} \end{pmatrix} = \underline{0}$$

\square

Discussion 1. In contrast to the cases $k = 0, 1$, the UTCBCs $\underline{u}(k)$ for $k = 2$ can negatively affect the minimum distance d_Z . As an example, consider the cycle \mathbf{C} in H_Γ highlighted in red in Example 4. The cycle \mathbf{C} corresponds to a square matrix of size L :

$$\begin{pmatrix} \text{3F} & & & \text{F1} \\ & \text{4C} & & 78 \\ & & \text{E1} & \text{89} \\ \text{8C} & & 16 & \\ & \text{A4} & & \text{85} \\ \text{F3} & & & \text{D4} \end{pmatrix}$$

In this instance, the matrix \mathbf{C} happens to be of full rank, and hence the associated subcode $N(\mathbf{C}; H_\Gamma)$ is the trivial (zero-dimensional) subspace consisting only of the all-zero codeword. That is, $N(\mathbf{C}; H_\Gamma) = \{\underline{0}\}$. However, if the arrangement of nonzero symbols in H_Γ were unfortunate and \mathbf{C} failed to be full rank, then $N(\mathbf{C}; H_\Gamma)$ would become a one-dimensional subspace, containing a nonzero codeword. Such a codeword corresponds to an uncorrectable logical error and can degrade the minimum distance d_Z (see (13)).

Therefore, eliminating or carefully controlling UTCBCs $\underline{u}(2)$ is crucial for ensuring that the minimum distance remains large.

V Proposed Code Construction

This section proposes an improved construction of the matrices \hat{H}_X , \hat{H}_Z , H_Γ , H_Δ , H_X and H_Z , based on the observations made in the previous section.

As shown in Theorem 3, the conventional codes presented in [31] inevitably contain length- $2L$ cycles \mathbf{C} that belong to the UTCBCs $\underline{u}(k)$ for $k \in \{0, 1, 2\}$. Among these, cycles in $\underline{u}(0)$ and $\underline{u}(1)$ are harmless to the minimum distance of the code, as established in Theorem 5. In contrast, as explained in Discussion 1, cycles in UTCBC $\underline{u}(2)$ may introduce low-weight codewords, depending on the specific values of the nonzero entries along the cycle, and therefore can degrade the minimum distance of C_Γ . The same argument applies to H_Δ by symmetry, by interchanging the roles of H_Γ and H_Δ .

In a related work [34], the error floor was successfully reduced for a code with $L = 8$ and rate $R = 1/2$ by eliminating all length- $2L$ cycles. However, for the target parameters considered in this paper, namely $J = 2$, $L = 6$ and $R = 1/3$, length- $2L$ cycles in UTCBCs are unavoidable due to Theorem 3.

TABLE II: Constructed $f_i(X)$ and $g_i(X)$ polynomials for each P

P	$f_0(X)$	$f_1(X)$	$f_2(X)$	$g_0(X)$	$g_1(X)$	$g_2(X)$
$384 = 2^7 \cdot 3$	$221X + 358$	$101X + 314$	$217X + 92$	$199X + 303$	$169X + 324$	$343X + 375$
$768 = 2^8 \cdot 3$	$235X + 723$	$127X + 345$	$277X + 6$	$565X + 374$	$725X + 166$	$709X + 366$
$1536 = 2^9 \cdot 3$	$1003X + 723$	$91X + 219$	$1045X + 6$	$1333X + 1142$	$65X + 1248$	$473X + 1012$
$3072 = 2^{10} \cdot 3$	$2155X + 1773$	$1165X + 1110$	$1237X + 2010$	$2957X + 1238$	$1885X + 638$	$2425X + 2908$
$6144 = 2^{11} \cdot 3$	$1099X + 1665$	$5875X + 69$	$1153X + 5952$	$2957X + 974$	$2173X + 4838$	$1973X + 2386$
$6500 = 2^2 \cdot 5^3 \cdot 13;$	$1X + 2998$	$1501X + 3518$	$5501X + 2346$	$3251X + 4459$	$3251X + 3900$	$1X + 988$
$12288 = 2^{12} \cdot 3$	$3433X + 3987$	$10801X + 9018$	$10177X + 6408$	$6065X + 5770$	$3169X + 2932$	$10193X + 8070$

V-A Guiding Principles for the Construction

The objective of this section is to refine the conventional construction method of [31] (see Section III) so that the resulting codes satisfy the following three properties:

- 1) The matrices \hat{H}_X and \hat{H}_Z contain no cycles of length less than $2L$.
- 2) All length- $2L$ cycles in \hat{H}_X and \hat{H}_Z belong to one of the UTCBCs $\underline{u}(k)$ with $k \in \{0, 1, 2\}$.
- 3) For all length- $2L$ cycles C belonging to the UTCBC $\underline{u}(2)$ in H_Γ and H_Δ , the null spaces $N(C; H_\Gamma)$ and $N(C; H_\Delta)$ are equal to $\{0\}$, respectively. In other words, each such cycle C must have full rank L (see Discussion 1).

Although eliminating all length-12 cycles requires $L \geq 8$ (see Theorem 3), our goal is to achieve robust performance even when $L = 6$ by carefully managing the structure and impact of UTCBCs.

In this section, we explicitly construct permutations \underline{f} and \underline{g} , along with the associated matrices \hat{H}_X , \hat{H}_Z , H_Γ , and H_Δ . Our goal is not merely to construct a single pair (\hat{H}_X, \hat{H}_Z) that satisfies the required conditions, but rather to randomly sample such pairs from the space of all valid constructions. This randomized approach is essential for harnessing the performance advantages of LDPC codes viewed as random codes [9].

In Section IV, we investigated the structural properties of the conventional construction over a broad class of permutations, assuming that \underline{f} and \underline{g} are drawn from general subsets of \mathcal{F}_P . Although it is difficult to randomly generate permutations from \mathcal{F}_P that satisfy the necessary conditions, the construction becomes significantly more efficient by leveraging the algebraic structure of APMs. While exploring the full class \mathcal{F}_P may offer greater randomness and potentially better-performing codes, we restrict ourselves to the structured subset $\mathcal{A}_P \subset \mathcal{F}_P$ to ensure algorithmic feasibility. Therefore, in the remainder of this paper, we focus on permutations selected from \mathcal{A}_P .

V-B Construction of \hat{H}_X and \hat{H}_Z

In this section, we aim to construct a pair of arrays of APMs

$$\underline{f} = (f_0, f_1, \dots, f_{L/2-1}), \quad \underline{g} = (g_0, g_1, \dots, g_{L/2-1}),$$

that satisfy the following criteria:

- (a) Each pair (f_i, g_i) must satisfy the commutativity condition specified in Requirement 1.
- (b) To prevent the formation of 2×3 totally closed block cycles (see Theorem 1), complete commutativity among the f_i 's or among the g_i 's must be avoided. Specifically, for some $i \neq j$, the permutations f_i and f_j should not commute, and likewise for g_i and g_j .
- (c) Other than the UTCBCs $\underline{u}(k)$ for $k \in \{0, 1, 2\}$, no additional closed block cycles of length at most $2L$ should appear in either \hat{H}_X or \hat{H}_Z .

Note. Although condition (b) may appear to be implied by condition (c), it plays a crucial role in the construction process. In practice, if condition (b) is not explicitly enforced, it becomes extremely difficult to find sequences that satisfy condition (c) via random sampling. We do not explicitly include Requirement 2 in the above criteria, since it is automatically satisfied once condition (c) holds.

To construct such APMs \underline{f} and \underline{g} , we employ a sequential randomized algorithm that incrementally builds each sequence by adding one APM at a time while checking the required constraints. Starting from an empty list, candidates for f_i and g_i are iteratively sampled from \mathcal{A}_P and evaluated to ensure that the resulting partial sequences satisfy conditions (a), (b), and (c). If a candidate satisfies all constraints, it is accepted and appended to the sequence; otherwise, a new candidate is drawn. This process is repeated until valid sequences \underline{f} and \underline{g} of length $L/2$ are obtained. The full procedure is detailed in Algorithm 1.

Using the APMs \underline{f} and \underline{g} determined by Algorithm 1, we compute the binary matrices \hat{H}_X and \hat{H}_Z .

Algorithm 1 Construction Algorithm of f and g

```

1: Initialize empty list  $\mathcal{S} \leftarrow []$ 
2: for  $i = 0$  to  $L/2 - 1$  do
3:   repeat
4:     Randomly generate a candidate  $f_i$  from  $\mathcal{A}_P$ 
5:     Temporarily set  $\mathcal{S}' \leftarrow \mathcal{S} \cup \{f_i\}$ 
6:     if  $\mathcal{S}'$  does not violate the criteria (a),(b), or (c) then
7:       Accept  $f_i$ :  $\mathcal{S} \leftarrow \mathcal{S}'$ 
8:       break
9:     end if
10:    until a valid  $f_i$  is found
11:   repeat
12:     Randomly generate a candidate  $g_i$  from  $\mathcal{A}_P$ 
13:     Temporarily set  $\mathcal{S}' \leftarrow \mathcal{S} \cup \{g_i\}$ 
14:     if  $\mathcal{S}'$  does not violate the criteria (a),(b), or (c) then
15:       Accept  $g_i$ :  $\mathcal{S} \leftarrow \mathcal{S}'$ 
16:       break
17:     end if
18:    until a valid  $g_i$  is found
19:  end for
20: return  $\mathcal{S}$ 

```

V-C Determination of H_Γ and H_Δ

In the previous section, we constructed matrices \hat{H}_X and \hat{H}_Z that satisfy Properties 1 and 2 listed in Section V-A. In this section, we aim to construct orthogonal matrices H_Γ and H_Δ that share the same support as \hat{H}_X and \hat{H}_Z , respectively, and satisfy Property 3 stated in Section V-A. Formally, in addition to the orthogonality conditions (9) and (10), we seek vector representations $\underline{\gamma}$ and $\underline{\delta}$ of H_Γ and H_Δ over \mathbb{F}_q that satisfy the following constraints:

$$A_2 \log \underline{\gamma} := \left[-\hat{H}_Z^{(2,L)} \mid \hat{H}_Z^{(2,R)} \mid \hat{H}_Z^{(2,L)} \mid -\hat{H}_Z^{(2,R)} \right] \log \underline{\gamma} = \underline{c} \pmod{q-1}, \quad (21)$$

$$B_2 \log \underline{\delta} := \left[-\hat{H}_X^{(2,L)} \mid \hat{H}_X^{(2,R)} \mid \hat{H}_X^{(2,L)} \mid -\hat{H}_X^{(2,R)} \right] \log \underline{\delta} = \underline{d} \pmod{q-1}, \quad (22)$$

where $c_i \neq 0$ and $d_i \neq 0$ for all $i \in [P]$. These constraints are derived in Appendix E. Each system consists of P equations in $2N$ variables, specifically the entries γ_i and δ_i for $i = 0, 1, \dots, 2N-1$.

By performing Gaussian elimination, we can obtain a solution $\log \underline{\gamma}$ that satisfies $A_{01} \log \underline{\gamma} = \underline{0}$. In this process, we decompose the vector $\log \underline{\gamma}$ satisfying (9), i.e., $A_{01} \log \underline{\gamma} = \underline{0}$, into a bound part and a free part, denoted as $\log \underline{\gamma} = (\log \underline{\gamma}_b \mid \log \underline{\gamma}_f)$. Let G_{01} be the linear transformation from the free part to the bound part:

$$\log \underline{\gamma}_b = G_{01} \log \underline{\gamma}_f, \quad (23)$$

where G_{01} is a matrix over \mathbb{Z}_{q-1} , and B and F denote the lengths of the bound and free parts, respectively.

We employ the following two randomized algorithms—Algorithm 2 and Algorithm 3—to construct the parity-check matrices H_Γ and H_Δ , respectively, with the desired properties.

Algorithm 2 constructs a matrix H_Γ such that $A_{01} \log \underline{\gamma} = \underline{0}$ and $A_2 \log \underline{\gamma}$ contains no zero entries. The algorithm begins by randomly generating the free part $\log \underline{\gamma}_f$ and computing the corresponding bound part $\log \underline{\gamma}_b$ using (23). Next, we compute a \mathbb{Z}_{q-1} -valued vector $\underline{c}^{(0)} := A_2 \log \underline{\gamma}$ of length P . If all entries of $\underline{c}^{(0)}$ are nonzero, then the corresponding vector $\underline{\gamma}$ is accepted. The vector $\underline{c}^{(0)}$ has P entries, each of which becomes zero with probability $1/(q-1)$. In this work, we set $q = 2^e$ with $e = 8$, so while the probability of a zero entry is small, such entries do occasionally occur. If any entry of $\underline{c}^{(0)}$ is zero, the algorithm perturbs a single free variable involved in the zero entry and updates the bound part accordingly. This process is repeated until all entries of $A_2 \log \underline{\gamma}$ are nonzero.

Given $\underline{\gamma}$, or equivalently H_Γ , Algorithm 3 constructs a matrix H_Δ such that $H_\Gamma H_\Delta^\top = \underline{0}$ and $B_2 \log \underline{\delta}$ contains no zero entries. As a first step, the algorithm solves the linear equation $H_\Gamma H_\Delta^\top = \underline{0}$ and randomly generates one valid solution for H_Δ . Next, we compute $\underline{d}^{(0)} := B_2 \log \underline{\delta}$. If any zero entry in $\underline{d}^{(0)}$ is detected, the algorithm perturbs a free variable in $\log \underline{\gamma}_f$, recomputes the bound part $\log \underline{\gamma}_b$, and updates H_Δ accordingly. This process continues until $B_2 \log \underline{\delta}$ is fully nonzero.

This paragraph discusses a trade-off in the proposed code construction between the probability of satisfying algebraic constraints and the decoding complexity. Assuming that the \mathbb{F}_q -valued labels assigned to each cycle are independently

Algorithm 2 Construction of H_Γ such that $A_2 \log \underline{\gamma} = 0$ and $A_2 \log \underline{\gamma}$ is nonzero in all entries

- 1: Randomly generate $\log \underline{\gamma}_f \in \mathbb{Z}_{q-1}^F$
- 2: Compute $\log \underline{\gamma}_b \leftarrow G_{01} \log \underline{\gamma}_f$
- 3: Compute $\underline{c}^{(0)} \leftarrow A_2 \log \underline{\gamma}$
- 4: **if** all entries of $\underline{c}^{(0)}$ are nonzero **then**
- 5: **return** H_Γ and terminate
- 6: **end if**
- 7: $i \leftarrow 0$
- 8: **while** true **do**
- 9: Randomly select and perturb a free variable γ_j in $\underline{\gamma}_f$
- 10: Recompute $\log \underline{\gamma}_b \leftarrow G_{01} \log \underline{\gamma}_f$
- 11: Compute $\underline{c}^{(i+1)} \leftarrow A_2 \log \underline{\gamma}$
- 12: **if** all entries of $\underline{c}^{(i+1)}$ are nonzero **then**
- 13: **return** H_Γ
- 14: **else if** the number of zeros in $\underline{c}^{(i+1)}$ is greater than or equal to that in $\underline{c}^{(i)}$ **then**
- 15: Undo the change to γ_j
- 16: **end if**
- 17: $i \leftarrow i + 1$
- 18: **end while**

Algorithm 3 Construction of H_Δ such that $H_\Gamma H_\Delta^\top = O$ and $B_2 \log \underline{\delta}$ is nonzero in all entries

- 1: Solve $H_\Gamma H_\Delta^\top = O$ and randomly generate one solution H_Δ
- 2: Compute $\underline{d}^{(0)} \leftarrow B_2 \log \underline{\delta}$
- 3: **if** all entries of $\underline{d}^{(0)}$ are nonzero **then**
- 4: **return** H_Δ and terminate
- 5: **end if**
- 6: $i \leftarrow 0$
- 7: **while** true **do**
- 8: Randomly perturb one free variable γ_j in $\underline{\gamma}_f$
- 9: Recompute $\log \underline{\gamma}_b \leftarrow G_{01} \log \underline{\gamma}_f$
- 10: Solve $H_\Gamma H_\Delta^\top = O$ and randomly generate one solution H_Δ
- 11: Compute $\underline{c} \leftarrow A_2 \log \underline{\gamma}$
- 12: Compute $\underline{d}^{(i+1)} \leftarrow B_2 \log \underline{\delta}$
- 13: **if** \underline{c} contains any zero entries **or** the number of zeros in $\underline{d}^{(i+1)}$ is greater than or equal to those in $\underline{d}^{(i)}$ **then**
- 14: Undo the change to γ_j
- 15: **else if** all entries of $\underline{d}^{(i+1)}$ are nonzero **then**
- 16: **return** H_Δ
- 17: **end if**
- 18: $i \leftarrow i + 1$
- 19: **end while**

and uniformly drawn at random, the probability that a single cycle in the UTCBC $u(2)$ is full rank is $1 - 1/q$, which increases with q . Since there are P such cycles, and assuming their labels are independently assigned, the probability that all of them are full rank is $(1 - 1/q)^P$. Thus, increasing q improves the chance that all cycles are full rank, whereas increasing P reduces it. On the other hand, the decoding complexity of the joint BP algorithm is proportional to q^2 . This is specifically required in the message updates in equations (34) and (35). As $q = 2^e$, the complexity grows rapidly with increasing e . This creates a practical constraint: while a larger q improves the algebraic robustness of the code, it also significantly increases decoding cost. Therefore, to keep the decoder complexity manageable, q must be kept reasonably small, which in turn limits how large P can be chosen in the construction.

V-D Construction of H_X and H_Z from \hat{H}_Γ and \hat{H}_Δ

Finally, the binary parity-check matrices H_X and H_Z are constructed from the non-binary matrices H_Γ and H_Δ in the same manner as described in Section III-C. Specifically, each entry $\gamma_{ij} \in \mathbb{F}_q$ in H_Γ is mapped to a binary $e \times e$ matrix $A(\gamma_{ij})$ using the companion matrix representation, and similarly, each entry $\delta_{ij} \in \mathbb{F}_q$ in H_Δ is mapped to $A(\delta_{ij})^\top$. This yields the binary matrices H_X and H_Z of size $m \times n$, where $m = eM$ and $n = eN$.

VI Joint Belief Propagation and Post-Processing Decoding

This section presents a decoding method designed to fully exploit the performance of the proposed codes described in the previous section. The primary goal is to concisely define a post-processing algorithm that enhances the conventional decoding method.

Section VI-A provides a general formulation of syndrome decoding using the binary vector representation of Pauli errors. Section VI-E defines the depolarizing channel, which serves as the physical noise model assumed in our numerical experiments. Section VI-B explains the degeneracy of quantum noise vectors and the conditions under which syndrome decoding can successfully recover the codeword. Section VI-C describes the joint) decoding algorithm over binary vectors, which serves as the basis of our approach. Section VI-D reformulates this decoding procedure over a finite field, enabling a more compact representation and facilitating the post-processing method. Section VI-E then analyzes the behavior of the conventional decoder in the error floor regime. Section VI-F presents an algorithm for estimating a set of cycles responsible for decoder stagnation. Finally, Section VI-G describes the proposed post-processing algorithm that refines the decoder output by solving a small linear system over the estimated support.

VI-A Pauli Channel and Binary Vector Representation of Errors

The Pauli group \mathcal{P}_n is non-commutative; however, by ignoring the global phase factor α of Pauli operators, we obtain the quotient group $\mathcal{P}_n/\{\pm I, \pm iI\}$, which is the subgroup $\{\pm I, \pm iI\} \subset \mathcal{P}_n$ modulo. Here, I represents the identity operator on the space \mathbb{C}^{2^n} , and $\alpha \in \{\pm 1, \pm i\}$ denotes a global phase factor that does not affect the measurement outcome of quantum states. This quotient group is isomorphic to the commutative group \mathbb{F}_2^{2n} , and the isomorphism for $E \in \mathcal{P}_n/\{\pm I, \pm iI\}$ is given as follows:

$$E = \alpha \bigotimes_{i=0}^{n-1} X^{x_i} Z^{z_i} \leftrightarrow (\underline{x} | \underline{z}) = (x_0, \dots, x_{n-1} | z_0, \dots, z_{n-1})^\top.$$

Using this correspondence, we identify the Pauli error E with its binary representation $(\underline{x} | \underline{z})$. Whether the vector is a row vector or column vector should be understood from the context.

A very important subclass of stabilizer codes [3] is the CSS codes [39], [40]. CSS codes are a type of stabilizer code characterized by the property that the non-identity components of each stabilizer generator within a tensor product are all equal to X or all equal to Z .

The check matrix of the stabilizer group S is expressed as binary vectors arranged in rows. Without loss of generality, the check matrix H of a CSS code of length n can be expressed as follows:

$$H = \begin{pmatrix} H_X & O \\ O & H_Z \end{pmatrix} \in \mathbb{F}_2^{(m_X + m_Z) \times 2n}, \quad (24)$$

where H_X, H_Z are binary matrices of sizes $m_X \times n$ and $m_Z \times n$, respectively. The commutativity of the stabilizer generators implies that $H_X H_Z^\top = O$. For simplicity, this paper assumes $m = m_X = m_Z$. The condition $H_X H_Z^\top = O$ is equivalent to the following:

$$C_Z^\perp \subset C_X, \quad C_X^\perp \subset C_Z, \quad (25)$$

where C_X, C_Z are the code spaces defined by H_X, H_Z when considered as parity-check matrices. Furthermore, the dimension k of the CSS code of length n can be determined by the following formula:

$$k = n - \text{rank } H_X - \text{rank } H_Z.$$

Let us consider the codeword state $|\psi\rangle$ with a Pauli error $E \leftrightarrow (\underline{x} | \underline{z})$ applied, resulting in the state $E|\psi\rangle$. The decoder considered in this paper performs decoding according to the following steps:

- 1) Measure the syndrome $(\underline{s} = H_Z \underline{x}, \underline{t} = H_X \underline{z}) \in \mathbb{F}_2^{2m}$.
- 2) Based on the syndrome, estimate the noise as $\hat{E} \leftrightarrow (\hat{\underline{x}} | \hat{\underline{z}})$ that satisfies the following:

$$H_X \hat{\underline{z}} = \underline{s}, \quad H_Z \hat{\underline{x}} = \underline{t} \quad (26)$$

- 3) The codeword $|\psi\rangle$ is affected by noise E , resulting in the state $E|\psi\rangle$. Applying \hat{E}^\dagger to this state yields $E^\dagger E|\psi\rangle$. If $\hat{E}^\dagger E \in S$, then $\hat{E}^\dagger E|\psi\rangle \propto |\psi\rangle$, and the codeword is recovered.

The condition $\hat{E}^\dagger E \in S$ is equivalent to the existence of $\underline{a} = (\underline{a}_X | \underline{a}_Z) = (a_0, \dots, a_{2m-1})^\top \in \mathbb{F}_2^{2m}$ such that

$$\prod_{i=0}^{2m-1} S_i^{a_i} = \hat{E}^\dagger E,$$

where S_i are the stabilizer generators for $i = 0, \dots, 2m - 1$. Moreover, since $\hat{E}^\dagger E \leftrightarrow (\underline{x} + \hat{\underline{x}} \mid \underline{z} + \hat{\underline{z}})$, this is equivalent to:

$$\sum_{i=1}^m a_i \underline{s}_i = (\underline{x} + \hat{\underline{x}} \mid \underline{z} + \hat{\underline{z}}), \quad \text{for } i = 1, \dots, m,$$

where $S_i \leftrightarrow \underline{s}_i$. Writing this in terms of matrices and vectors, we get $H^\top \underline{a} = (\underline{x} + \hat{\underline{x}} \mid \underline{z} + \hat{\underline{z}})$. Specifically, for CSS codes, since the parity-check matrix is given by (24), we use $\underline{a} = (\underline{a}_X \mid \underline{a}_Z)$ to obtain:

$$(H_X)^\top \underline{a}_X = \underline{x} + \hat{\underline{x}}, \quad (H_Z)^\top \underline{a}_Z = \underline{z} + \hat{\underline{z}}$$

which is equivalent to

$$G_X(\underline{x} + \hat{\underline{x}}) = 0, \quad G_Z(\underline{z} + \hat{\underline{z}}) = 0,$$

or equivalently,

$$\hat{\underline{x}} + \underline{x} \in C_X^\perp, \quad \hat{\underline{z}} + \underline{z} \in C_Z^\perp, \quad (27)$$

where G_X, G_Z are generator matrices of C_X, C_Z , respectively. From (25), it follows that (27) implies

$$H_X(\underline{z} + \hat{\underline{z}}) = 0, \quad H_Z(\underline{x} + \hat{\underline{x}}) = 0,$$

which is equivalent to (26).

We assume a depolarizing channel with physical error rate p_D . The hashing bound for the depolarizing channel with p_D is given by

$$1 - H_2(p_D) - p_D \log_2(3),$$

where $H_2(\cdot)$ is the binary entropy function. In this section, we describe the probability distribution of X and Z errors induced by the channel.

Let $M = PJ$, $N = PL$, and $n = eN$. For $n = eN$ qubits, the vector representations of X and Z errors are denoted by \underline{x} and \underline{z} , respectively. We divide \underline{x} and \underline{z} into e -bit segments and write

$$\underline{x} = (x_0, \dots, x_{N-1})^\top, \quad \underline{z} = (z_0, \dots, z_{N-1})^\top.$$

Each x_j and z_j is a binary vector of length e . The probability of occurrence for $\underline{x}, \underline{z} \in \mathbb{F}_2^{eN}$ in this channel is given by

$$\begin{aligned} p(\underline{x}, \underline{z}) &= \prod_{j=0}^{N-1} p(x_j, z_j), \\ p(x_j, z_j) &= \prod_{k=0}^{e-1} p(x_{j,k}, z_{j,k}), \\ p(x_{j,k}, z_{j,k}) &= \begin{cases} 1 - p_D, & (x_{j,k}, z_{j,k}) = (0, 0), \\ \frac{p_D}{3}, & (x_{j,k}, z_{j,k}) = (0, 1), (1, 0), (1, 1), \end{cases} \end{aligned}$$

where $x_{j,k}, z_{j,k} \in \mathbb{F}_2$ denote the k -th bit of x_j and z_j , respectively, for $k = 0, 1, \dots, e - 1$.

VI-B Degeneracy and Logical Correctness

The decoding process involves estimating the noise vectors $\underline{x}, \underline{z} \in \mathbb{F}_2^n$ from the syndromes $\underline{s}, \underline{t} \in \mathbb{F}_2^m$

$$\underline{s} = H_Z \underline{x} \text{ and } \underline{t} = H_X \underline{z}.$$

The decoder attempts to find a likely noise estimate $\hat{\underline{x}}$ and $\hat{\underline{z}}$ that satisfy

$$H_Z \hat{\underline{x}} = \underline{s}, \quad H_X \hat{\underline{z}} = \underline{t}, \quad (28)$$

that is, a vector consistent with the syndrome. Naturally, the true noise vectors \underline{x} and \underline{z} also satisfy this condition.

Such a vector $\hat{\underline{x}}$ and $\hat{\underline{z}}$ are not unique due to degeneracy: the number of solutions is equal to the size of the code C_Z . Indeed, Eq. (28) is equivalent to

$$\underline{x} + \hat{\underline{x}} \in C_Z, \quad \underline{z} + \hat{\underline{z}} \in C_X.$$

Hence, the set of all solutions can be written as a coset:

$$\underline{x} + C_Z = \{\underline{x} + \underline{x}' \mid \underline{x}' \in C_Z\}, \quad \underline{z} + C_X = \{\underline{z} + \underline{z}' \mid \underline{z}' \in C_X\}.$$

In classical communication, syndrome decoding aims to identify the exact noise vector; the estimate must match the true error. However, in quantum error correction, exact identification is not necessary. Instead, if the following condition holds:

$$\underline{x} + \hat{\underline{x}} \in C_X^\perp, \quad \underline{z} + \hat{\underline{z}} \in C_Z^\perp, \quad (29)$$

then a recovery operator constructed from $\hat{\underline{x}}$ and $\hat{\underline{z}}$ will correctly restore the quantum state, despite potential mismatches between the estimated and true noise vectors. An error that satisfies (28) but not (29), in other words,

$$\underline{x} + \hat{\underline{x}} \in C_Z \setminus C_X^\perp, \quad \underline{z} + \hat{\underline{z}} \in C_X \setminus C_Z^\perp,$$

is called a logical error, as it transforms the state into a different codeword state. That is, the recovery still satisfies the stabilizer constraints but results in a misidentification of the logical state.

VI-C Conventional Algorithm: Joint Belief Propagation Decoding over Binary Vectors

The idea of the joint BP decoding algorithm was, to the best of the authors' knowledge, proposed in [12]. Although the algorithm was not explicitly described in that work, it was later formulated as a message-passing algorithm in [31], or perhaps even earlier in other sources.

The algorithm is employed to simultaneously estimate the noise vectors \underline{x} and \underline{z} . In that formulation, the noise components x_j and z_j are treated as random variables over binary vectors, and the decoding algorithm is driven by a factorization of the joint posterior distribution. Specifically, the factor graph is constructed based on a function proportional to the posterior probability, which is used to guide the message passing in the BP decoder.

The posterior probability of $\underline{x}, \underline{z}$ given the syndromes $\underline{s}, \underline{t}$ can be sparsely factorized as follows:

$$\begin{aligned} p(\underline{x}, \underline{z} | \underline{s}, \underline{t}) &\propto \mathbb{1}[H_Z \underline{x} = \underline{s}] \mathbb{1}[H_X \underline{z} = \underline{t}] p(\underline{x}, \underline{z}) \\ &= \left(\prod_{i \in [M]} \mathbb{1}\left[\sum_{j \in [N]} (H_Z)_{ij} x_j = s_i \right] \right) \left(\prod_{i \in [M]} \mathbb{1}\left[\sum_{j \in [N]} (H_X)_{ij} z_j = t_i \right] \right) \left(\prod_{j \in [N]} p(x_j, z_j) \right), \end{aligned} \quad (30)$$

where $(H_X)_{ij}$ and $(H_Z)_{ij}$ denote the (i, j) -th $(e \times e)$ submatrices of H_X and H_Z , respectively. These submatrices are defined by the companion matrix mapping:

$$(H_X)_{ij} = A(\gamma_{ij}), \quad (H_Z)_{ij} = A(\delta_{ij})^\top,$$

where $\gamma_{ij}, \delta_{ij} \in \mathbb{F}_q$ are the entries of the non-binary parity-check matrices H_Γ and H_Δ , respectively, and $A(\cdot)$ denotes the $e \times e$ binary companion matrix associated with each field element in \mathbb{F}_q (see Appendices A and B for details).

We denote $\mathbb{1}[\cdot]$ as 1 if the inside the brackets is true, and 0 otherwise. For each i , note that there are L values of j for which $(H_X)_{ij}$ and $(H_Z)_{ij}$ are non-zero, respectively. In [31], this factorization was used to formulate the joint BP decoding algorithm.

VI-D Joint Belief Propagation Decoding over Finite Field

In the concluding part of Section VI, we will propose a post-processing technique for the joint BP algorithm. For the sake of a concise formulation, this section describes a joint BP algorithm over a finite field, which is equivalent to the one over binary vectors defined in Section VI-C.

For $x_j, z_j \in \mathbb{F}_2^e$, we define $\xi_j, \zeta_j \in \mathbb{F}_q$ such that

$$\underline{v}(\xi_j) = x_j \text{ and } \underline{w}(\zeta_j) = z_j, \quad (31)$$

respectively. Similarly, we define $\sigma_i, \tau_i \in \mathbb{F}_q$ such that $\underline{v}(\sigma_i) = \underline{s}_i$ and $\underline{w}(\tau_i) = \underline{t}_i$. Then, by Theorems 9 and 12 in the Appendices, we obtain the following equivalences:

$$\begin{aligned} H_\Delta \underline{\xi} = \underline{\sigma} &\iff H_Z \underline{x} = \underline{s}, \\ H_\Gamma \underline{\zeta} = \underline{\tau} &\iff H_X \underline{z} = \underline{t} \end{aligned} \quad \left. \right\}. \quad (32)$$

Using the equivalence in (32), the decoding constraint (30) in terms of binary variables $\underline{x}, \underline{z}$ can be equivalently rewritten using \mathbb{F}_q -valued variables $\underline{\xi}, \underline{\zeta} \in \mathbb{F}_q^N$ as follows:

$$\begin{aligned} p(\underline{x}, \underline{z} | \underline{s}, \underline{t}) &\propto \mathbb{1}[H_Z \underline{x} = \underline{s}] \mathbb{1}[H_X \underline{z} = \underline{t}] p(\underline{x}, \underline{z}) \\ &= \mathbb{1}[H_\Delta \underline{\xi} = \underline{\sigma}] \mathbb{1}[H_\Gamma \underline{\zeta} = \underline{\tau}] p(\underline{\xi}, \underline{\zeta}) \\ &= \left(\prod_{i \in [M]} \mathbb{1}\left[\sum_{j \in [N]} \delta_{ij} \xi_j = \sigma_i \right] \right) \left(\prod_{i \in [M]} \mathbb{1}\left[\sum_{j \in [N]} \gamma_{ij} \zeta_j = \tau_i \right] \right) \left(\prod_{j \in [N]} p(\xi_j, \zeta_j) \right) \\ &\stackrel{\text{def}}{=} p(\underline{\xi}, \underline{\zeta} | \underline{\sigma}, \underline{\tau}). \end{aligned} \quad (33)$$

Here, the pairwise prior $p(\xi_j, \zeta_j)$ is defined as $p(\xi_j, \zeta_j) \stackrel{\text{def}}{=} p(x_j, z_j)$ for a pair (x_j, z_j) satisfying the mapping condition described in (31).

The joint BP algorithm that marginalizes the posterior probability $p(\underline{\xi}, \underline{\zeta} | \underline{\sigma}, \underline{\tau})$ is an algorithm that updates the following eight types of messages:

$$\begin{aligned} \mu_{ij}^{(\ell),X}(\xi_j), \nu_{ji}^{(\ell),X}(\xi_j), \lambda_j^{(\ell),X}(\xi_j), \kappa_j^{(\ell),X}(\xi_j), \\ \mu_{ij}^{(\ell),Z}(\zeta_j), \nu_{ji}^{(\ell),Z}(\zeta_j), \lambda_j^{(\ell),Z}(\zeta_j), \kappa_j^{(\ell),Z}(\zeta_j), \end{aligned}$$

at the iteration round $\ell = 0, 1, \dots$. These messages are probability vectors of length q . Note that although we use Greek letters to denote these messages, they represent probability distributions and not elements of the finite field. The following messages are initialized to the uniform distribution over $\xi_j, \zeta_j \in \mathbb{F}_q$, respectively:

$$\begin{aligned} \lambda_j^{(0),X}(\xi_j) &= 1/q, \\ \lambda_j^{(0),Z}(\zeta_j) &= 1/q, \\ \nu_{ij}^{(0),X}(\xi_j) &= 1/q, \\ \nu_{ij}^{(0),Z}(\zeta_j) &= 1/q. \end{aligned}$$

Each message is updated at each iteration round $\ell = 0, 1, 2, \dots$ using the following update equations. After each update, the messages are normalized to ensure they form probability distributions.

$$\kappa_j^{(\ell),X}(\xi_j) = \sum_{\zeta_j} p(\xi_j, \zeta_j) \lambda_j^{(\ell),Z}(\zeta_j), \quad (34)$$

$$\kappa_j^{(\ell),Z}(\zeta_j) = \sum_{\xi_j} p(\xi_j, \zeta_j) \lambda_j^{(\ell),X}(\xi_j), \quad (35)$$

$$\mu_{ji}^{(\ell),X}(\xi_j) = \kappa_j^{(\ell),X}(\xi_j) \prod_{i' \in \partial_Z(j) \setminus i} \nu_{i'j}^{(\ell),X}(\xi_j),$$

$$\mu_{ji}^{(\ell),Z}(\zeta_j) = \kappa_j^{(\ell),Z}(\zeta_j) \prod_{i' \in \partial_X(j) \setminus i} \nu_{i'j}^{(\ell),Z}(\zeta_j),$$

$$\nu_{ij}^{(\ell+1),X}(\xi_j) = \sum_{(\xi_{j'}) : j' \in \partial_Z(i) \setminus j} \mathbb{1} \left[\sum_{j' \in \partial_Z(i)} \delta_{ij'} \xi_{j'} = \sigma_i \right] \prod_{j' \in \partial_Z(i) \setminus j} \mu_{j'i}^{(\ell),X}(\xi_{j'}), \quad (36)$$

$$\nu_{ij}^{(\ell+1),Z}(\zeta_j) = \sum_{(\zeta_{j'}) : j' \in \partial_X(i) \setminus j} \mathbb{1} \left[\sum_{j' \in \partial_X(i)} \gamma_{ij'} \zeta_{j'} = \tau_i \right] \prod_{j' \in \partial_X(i) \setminus j} \mu_{j'i}^{(\ell),Z}(\zeta_{j'}), \quad (37)$$

$$\lambda_j^{(\ell+1),X}(\xi_j) = \prod_{i \in \partial_Z(j)} \nu_{ij}^{(\ell+1),X}(\xi_j),$$

$$\lambda_j^{(\ell+1),Z}(\zeta_j) = \prod_{i \in \partial_X(j)} \nu_{ij}^{(\ell+1),Z}(\zeta_j),$$

where $\partial_X(i) \subset [N]$ and $\partial_Z(i) \subset [N]$ are the set of column index j such that $\gamma_{ij} \neq 0$ and $\delta_{ij} \neq 0$, respectively. Similarly, $\partial_X(j) \subset [M]$ and $\partial_Z(j) \subset [M]$ are the set of row index i such that $\gamma_{ij} \neq 0$ and $\delta_{ij} \neq 0$, respectively. It holds that $\#\partial_X(i) = \#\partial_Z(i) = L$ and $\#\partial_X(j) = \#\partial_Z(j) = J$. The outer summation in (36) is taken over all vectors $(\xi_{j'})$ of length $L - 1$, where $j' \in \partial_Z(i) \setminus \{j\}$ and each component $\xi_{j'}$ ranges over \mathbb{F}_q . In this summation, the variable ξ_j is fixed, and the sum is taken over all other variables involved in the parity check at node i . The interpretation of the summation in (37) is analogous, with ζ_j fixed and the summation taken over all $\zeta_{j'}$ for $j' \in \partial_X(i) \setminus \{j\}$.

We define the estimated noise at iteration ℓ as

$$\begin{aligned} \hat{\xi}_j^{(\ell)} &\stackrel{\text{def}}{=} \operatorname{argmax}_{\xi_j} \kappa_j^{(\ell),X}(\xi_j) \prod_{i \in \partial_Z(j)} \nu_{ij}^{(\ell),X}(\xi_j), \\ \hat{\zeta}_j^{(\ell)} &\stackrel{\text{def}}{=} \operatorname{argmax}_{\zeta_j} \kappa_j^{(\ell),Z}(\zeta_j) \prod_{i \in \partial_X(j)} \nu_{ij}^{(\ell),Z}(\zeta_j). \end{aligned}$$

At each iteration ℓ , we check whether these estimated syndromes match the true syndromes $\underline{\sigma}$ and $\underline{\tau}$. If both conditions $H_{\Delta} \hat{\xi}^{(\ell)} = \underline{\sigma}$ and $H_{\Gamma} \hat{\zeta}^{(\ell)} = \underline{\tau}$ are satisfied, then $\hat{\xi}^{(\ell)}$ and $\hat{\zeta}^{(\ell)}$ are accepted as the estimated noise, and the algorithm terminates. If either condition is not satisfied, the decoding continues.

The messages (36) and (37) can be computed using FFT [27], requiring $O(Lq \log q)$ operations per message. On the other hand the computation for messages (34) and (35) require $O(q^2)$ operations per message. Other messages computation require only $O(Jq)$ operations per message. Moreover, since the message updates at each node do not

share memory, they can be computed in parallel across all nodes. As performance improves with increasing P , and assuming q is fixed, the overall computational complexity is proportional to the number of physical qubits $n = ePL$. In the experiments conducted in this paper, we set $q = 2^e$ with $e = 8$.

Example 8. Based on the 16×48 binary matrices H_Γ and H_Δ given in Example 4, we illustrate the factor graph associated with Eq. (33), as shown in Fig. 1. The Tanner graphs on the left and right correspond to H_Δ and H_Γ , respectively. The edges that form the cycle included in the UTCBC presented in Example 4 are highlighted with thicker lines in their corresponding colors. Each side contains 16 parity-check nodes. The variable nodes representing the noise variables ξ_j and ζ_j are placed on each side, with 48 nodes per side. The central factor nodes represent the joint distribution $p(\xi_j, \zeta_j)$ of the noise variables. The directions of the messages passed along the edges are indicated at the bottom of the graph. \square

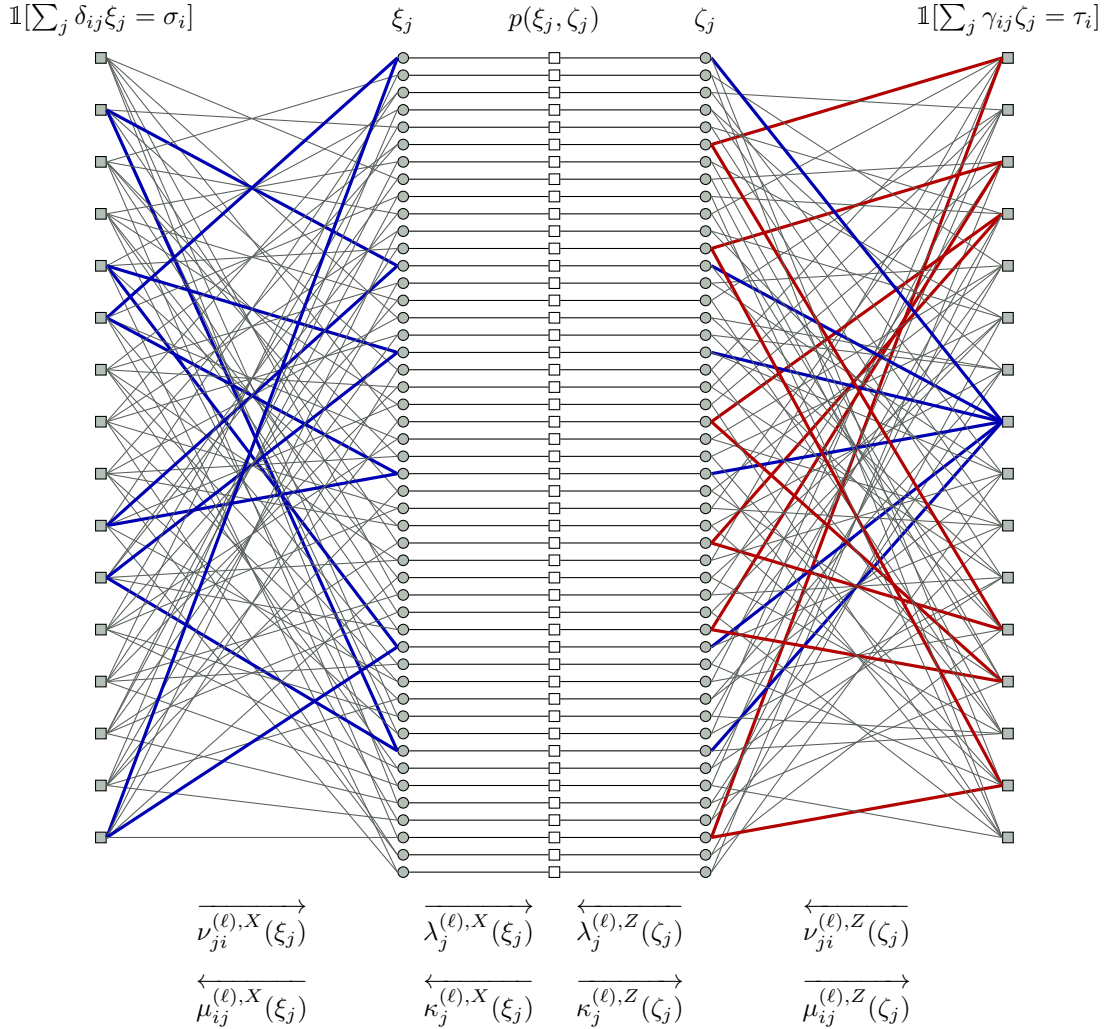


Fig. 1: Factor graph corresponding to Eq. (33). The joint BP algorithm can be interpreted as a message-passing algorithm executed on this graph. The directions of the messages are indicated by arrows.

Using the conventional code construction method described in Section III, we consider codes defined by (H_X, H_Z) , or equivalently (H_Γ, H_Δ) . Figure 2 shows the decoding performance by the conventional decoding method presented in Section VI-D. In this experiment, degeneracy was not taken into account, and decoding is considered successful only when the estimated noise exactly matches the true noise, i.e., $(\hat{\xi} = \xi, \hat{\zeta} = \zeta)$. For codes with $L \geq 8$ and rate $R \geq 0.5$, no significant error floor is observed, and the performance approaches the hashing bound. On the other hand, for $L = 6$ and rate $R = 1/3$, a high error floor emerges as the code length increases. In the next section, we discuss the structural properties of the codes that lead to this error floor.

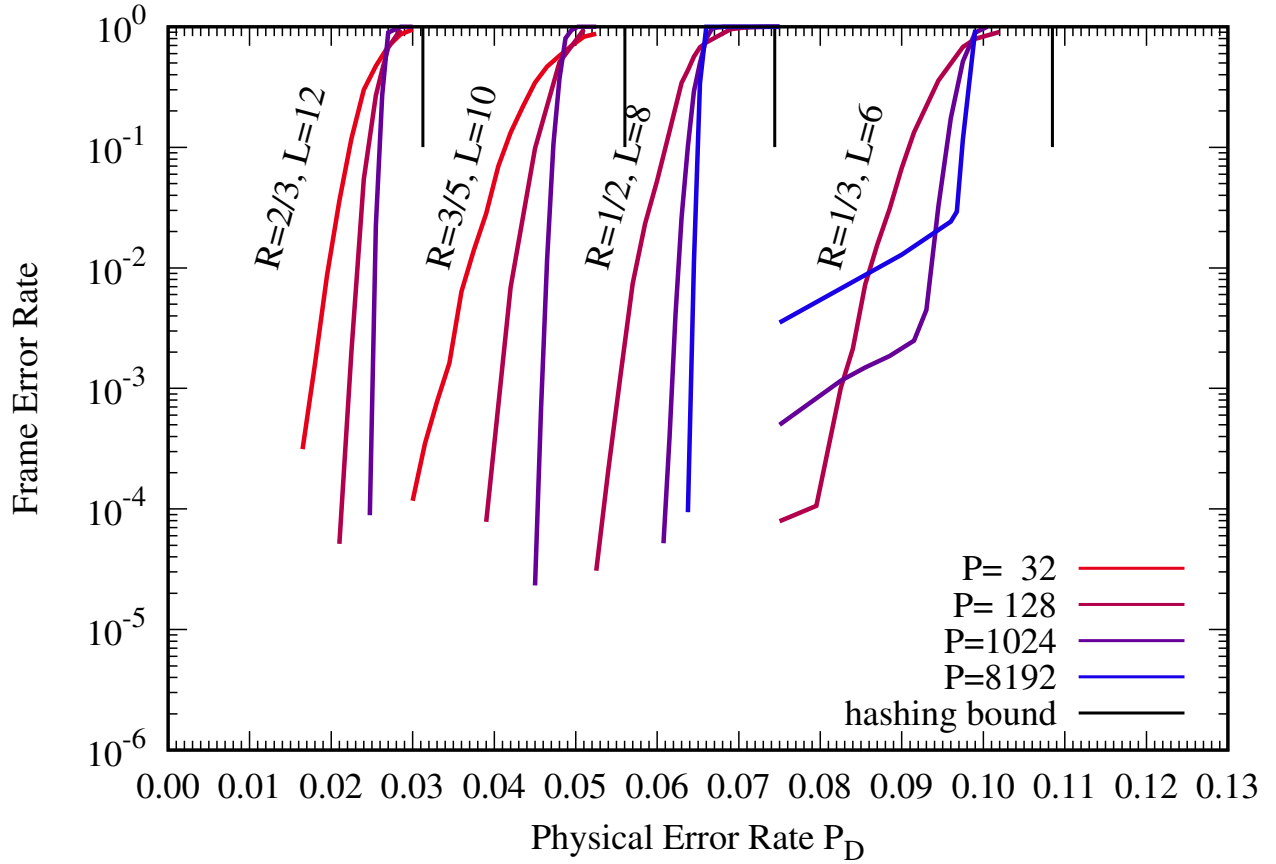


Fig. 2: Decoding performance of the conventional decoder applied to the conventional code proposed in [31] for several row weights L and coding rates $R = 1 - 2J/L$. The field size is $q = 2^e$ with $e = 8$, and the number of physical qubits is given by $n = eN = ePL$. When $L > 6$ and $R > 1/3$, no observable error floor appears down to a frame error rate (FER) of 10^{-4} as the blocklength increases. In contrast, for $L = 6$ and $R = 1/3$, a pronounced error floor emerges as the blocklength increases.

VI-E Observations of Decoder Behavior in the Error Floor Regime

To characterize the typical behavior of the joint BP algorithm in the error floor regime, we begin by defining the following metrics. The decoder attempts to find the noise vector estimates $\hat{\underline{\xi}}$ and $\hat{\zeta}$ such that

$$\underline{\sigma} = H_{\Delta}\hat{\underline{\xi}} \text{ and } \underline{\tau} = H_{\Gamma}\hat{\zeta}.$$

In the following, we focus on the estimation of X -noise $\hat{\underline{\xi}}$. The estimation of Z -noise $\hat{\zeta}$ can be handled in an analogous manner.

For the output of the joint BP algorithm at the ℓ -th iteration, the set of indices at which the estimated noise $\hat{\underline{\xi}}^{(\ell)}$ is incorrect is defined by

$$K_{\text{err}}^{(\ell)} = \{j \in [N] \mid \hat{\xi}_j^{(\ell)} \neq \xi_j\}.$$

Similarly, we define the set of unsatisfied syndrome check indices as

$$I_{\text{err}}^{(\ell)} = \{i \in [M] \mid \underline{\sigma}_i^{(\ell)} = H_{\Delta}\hat{\underline{\xi}}^{(\ell)}, \sigma_i^{(\ell)} \neq \sigma_i\}.$$

Next, we define the set of variable nodes whose estimated values have changed at least once during the last d iterations, denoted by $K_d^{(\ell)}$. Specifically,

$$K_d^{(\ell)} = \{j \in [N] \mid \hat{\xi}_j^{(\ell'-1)} \neq \hat{\xi}_j^{(\ell')} \text{ for some } \ell' \in [\ell - d, \ell]\}. \quad (38)$$

We define the set of syndrome indices that have changed at least once during the last d iterations as

$$I_d^{(\ell)} = \{i \in [M] \mid \underline{\sigma}_i^{(\ell')} = H_{\Delta}\hat{\underline{\xi}}^{(\ell')}, \sigma_i^{(\ell')} \neq \sigma_i \text{ for some } \ell' \in [\ell - d, \ell]\}.$$

TABLE III: Decoding Statistics over Iterations for $J = 2, L = 6, P = 6500, N = LP = 39000, M = JP = 13000, p_D = 9.435\%$ and $d = 8$.

ℓ	Estimation for ξ				Estimation for ζ			
	$ K_{\text{err}}^{(\ell)} $	$ K_d^{(\ell)} $	$ I_{\text{err}}^{(\ell)} $	$ I_d^{(\ell)} $	$ K_{\text{err}}^{(\ell)} $	$ K_d^{(\ell)} $	$ I_{\text{err}}^{(\ell)} $	$ I_d^{(\ell)} $
0	14944	0	9689	9689	15017	0	9741	9741
1	13731	4270	8618	10371	13845	4165	8677	10399
2	12875	6986	7676	10631	12959	6864	7791	10656
3	12108	8776	7036	10757	12306	8660	7178	10791
4	11693	10053	6558	10852	11765	10017	6717	10883
5	11297	11035	6221	10907	11370	11022	6304	10941
6	10866	11808	5862	10951	11043	11808	6028	10986
7	10542	12446	5640	10974	10667	12518	5745	11027
8	10300	12950	5464	10044	10364	13119	5537	10141
9	10069	11536	5216	9337	10099	11796	5334	9442
:	:	:	:	:	:	:	:	:
41	466	5682	462	3625	846	5956	684	3755
42	221	5088	204	3167	473	5405	436	3421
43	90	4337	103	2742	227	4822	225	3053
44	15	3633	25	2307	81	4243	95	2664
45	2	2980	2	1856	21	3575	27	2210
46	3	2257	4	1389	5	2882	7	1755
47	2	1595	2	909	0	2197	0	1300
48	2	973	2	565	0	1538	0	897
49	3	538	4	261	0	998	0	531
50	2	250	2	118	0	542	0	264
51	2	101	2	29	0	256	0	108
52	3	19	4	6	0	87	0	30
53	2	6	2	6	0	23	0	7
54	2	6	2	6	0	5	0	0
55	3	6	4	6	0	0	0	0
56	2	6	2	6	0	0	0	0
57	2	6	2	6	0	0	0	0
58	3	6	4	6	0	0	0	0
:	:	:	:	:	:	:	:	:

Note that among the quantities defined above, the decoder cannot directly observe $K_{\text{err}}^{(\ell)}$. In contrast, all the other variables— $K_d^{(\ell)}$, $I_{\text{err}}^{(\ell)}$, and $I_d^{(\ell)}$ —can be computed from the internal state and history of the joint BP decoder.

Table III provides an example of a decoding state transition. The example is based on a code constructed by the proposed method and decoded using the conventional joint BP algorithm over a depolarizing channel with physical error rate $p_D = 9.435\%$. Further details are provided in Section VII-B. The performance for other values of p_D is shown as the solid blue curve in Fig. 3. The decoder is applied to a code with parameters $J = 2, L = 6$, and $P = 6500$, and aims to estimate both ξ and ζ .

In the estimation of Z-noise vector ζ , the sizes of $K_{\text{err}}^{(\ell)}$ and $I_{\text{err}}^{(\ell)}$ both decrease monotonically to zero as the iteration index ℓ increases. The decoder successfully estimates the noise at iteration $\ell = 47$. Although typical cases exhibit similar success in estimating X-noise vector ξ , this particular example illustrates a rare failure of joint BP decoding to correctly estimate the noise vector ξ , occurring with probability on the order of 10^{-2} .

In the estimation of ξ , the sizes of $K_{\text{err}}^{(\ell)}$ and $I_{\text{err}}^{(\ell)}$ initially decrease monotonically. However, at a certain point, this decrease stagnates: although the number of incorrect estimates continues to decline, a small number of errors persist and never vanish, even after additional iterations. In this example, as ℓ increases, both $K_d^{(\ell)}$ and $I_d^{(\ell)}$ converge to a fixed set of size six. Within these sets, the values of $K_{\text{err}}^{(\ell)}$ and $I_{\text{err}}^{(\ell)}$ continue to fluctuate across iterations.

$$\begin{aligned} K_d^{(\ell)} &= \{[4062, 0]_L, [10410, 1]_L, [13890, 2]_L, [25420, 0]_R, [31699, 1]_R, [35508, 2]_R\}, \\ I_d^{(\ell)} &= \{[2853, 0], [2922, 0], [3490, 0], [6662, 1], [9201, 1], [12902, 1]\}. \end{aligned}$$

The numbers in parentheses indicate the corresponding block index for each variable or check node.

We examined the positions of the six variable nodes that failed to be correctly decoded and the corresponding unsatisfied check nodes in the matrix H_Δ . Specifically, we analyzed the submatrix of H_Δ formed by the rows indexed

by $I_{\text{err}}^{(\ell)}$ and the columns indexed by $K_{\text{err}}^{(\ell)}$. The entries of this submatrix are as follows:

$$\begin{array}{cccccc}
 & [4062, 0]_L & [10410, 1]_L & [13890, 2]_L & [25420, 0]_R & [31699, 1]_R & [35508, 2]_R \\
 [2853, 0] & \alpha^{77} & 0 & 0 & 0 & \alpha^{79} & 0 \\
 [2922, 0] & 0 & \alpha^{119} & 0 & \alpha^{168} & 0 & 0 \\
 [3490, 0] & 0 & 0 & \alpha^{179} & 0 & 0 & \alpha^{235} \\
 [6662, 1] & \alpha^{65} & 0 & 0 & 0 & 0 & \alpha^{145} \\
 [9201, 1] & 0 & \alpha^{121} & 0 & 0 & \alpha^{174} & 0 \\
 [12902, 1] & 0 & 0 & \alpha^{92} & \alpha^{66} & 0 & 0
 \end{array}$$

Here, the notations $[i, b] = bP + i$, $[i, b]_L = bP + i$, and $[i, b]_R = (b + L/2)P + i$ are the same as those introduced in the proof of Theorem 4. This submatrix forms a cycle of length 12 ($= 2L$). From the order in which the blocks appear, we can identify this as a Tanner cycle belonging to an unavoidable TCBC $\underline{u}(1)$ in H_Δ .

We have also observed other failure patterns, such as compound graphs formed by two length-12 cycles, or configurations trapped in length-16 cycles composed of 8×8 submatrices, which occur with a probability roughly two orders of magnitude lower. The objective of this section is to propose a post-processing algorithm that rescues the joint BP decoder from such cycle-induced failures where decoding does not succeed due to being trapped in one or more cycles.

In the remainder of this section, we consider a scenario in which the estimate of the X-noise has not yet converged—namely, it is trapped in a combination of a few length-12 cycles resulting in

$$H_\Delta \hat{\xi}^{(\ell)} \neq \underline{\alpha}.$$

Failures in estimating Z-noise can be handled in a symmetric manner.

Let $\mathcal{C}^{(2L)}$ denote the set of all Tanner cycles of length $2L$ contained in H_Δ (the definition for H_Γ is analogous). Based on Condition 2 in Section V-A, the matrix H_Δ constructed by the proposed method is designed so that all such cycles belong to the unavoidable TCBCs $\underline{u}(k)$ for $k \in \{0, 1, 2\}$. In other words, $\mathcal{C}^{(2L)}$ consists solely of the Tanner cycles contained in the unavoidable TCBCs $\underline{u}(k)$ for $k \in \{0, 1, 2\}$. Since there are P cycles for each value of k , the total number of such cycles is $3P$, and hence the size of $\mathcal{C}^{(2L)}$ is $3P$.

For a cycle $\mathbf{C} \in \mathcal{C}^{(2L)}$ of length $2L$, let $K(\mathbf{C})$ and $I(\mathbf{C})$ denote its column index set and row index set, respectively. For a collection \mathcal{C} of such cycles, we define the combined column and row index sets as

$$\begin{aligned}
 K(\mathcal{C}) &\triangleq \bigcup_{\mathbf{C} \in \mathcal{C}} K(\mathbf{C}) = K\left(\bigcup_{\mathbf{C} \in \mathcal{C}} \mathbf{C}\right), \\
 I(\mathcal{C}) &\triangleq \bigcup_{\mathbf{C} \in \mathcal{C}} I(\mathbf{C}) = I\left(\bigcup_{\mathbf{C} \in \mathcal{C}} \mathbf{C}\right).
 \end{aligned}$$

We say that joint BP at iteration ℓ or the estimated noise $\hat{\xi}^{(\ell)}$ is *trapped* in the union of cycles $\mathcal{C} \subset \mathcal{C}^{(2L)}$ if the following holds:

$$K_{\text{err}}^{(\ell)} \subset K(\mathcal{C}). \quad (39)$$

That is, all indices where the estimated noise is incorrect lie within the column support of the cycles in \mathcal{C} , that is,

$$\xi_j^{(\ell)} \neq \hat{\xi}_j^{(\ell)} \implies j \in K(\mathcal{C}).$$

Conversely, all indices outside $K(\mathcal{C})$ correspond to correctly estimated noise values, that is,

$$j \notin K(\mathcal{C}) \implies \xi_j^{(\ell)} = \hat{\xi}_j^{(\ell)}.$$

In [35], only the special case where \mathcal{C} consists of a single cycle (i.e., $|\mathcal{C}| = 1$) was considered.

In the error floor region, experiments using the conventional decoding method on the proposed codes revealed the following observation: when the decoder stagnated, the estimated noise was typically trapped in the union of a small number of cycles, most of which had length $2L$, and occasionally of length $2(L+2)$ with low probability. In this work, we focus on the case where the estimated noise is trapped in a union of length- $2L$ cycles, and propose a post-processing method to address this situation. In the next section, we address the problem of estimating the set of cycles in which the decoder becomes stuck and trapped during decoding.

VI-F Estimation of the Cycle Set \mathcal{C}

In this section, we describe an algorithm for estimating a minimal subset $\mathcal{C} \subset \mathcal{C}^{(2L)}$ that satisfies condition (39), to be applied when the joint BP decoder stagnates after failing to find a noise estimate that satisfies the syndrome condition. Naturally, the decoder does not have access to the true noise ξ or to the set $K_{\text{err}}^{(\ell)}$ of misestimated indices. Instead, we

use $K_d^{(\ell)}$, the set of variable nodes whose estimated values have changed during the last d iterations (see (38)), which can be computed by the decoder. Based on $K_d^{(\ell)}$, we estimate the cycle set \mathcal{C} according to the following strategy:

- 1) If $K_d^{(\ell)}$ and $K(\mathcal{C})$ share at least two elements, then include \mathcal{C} in $\hat{\mathcal{C}}$.
- 2) Limit the number of cycles in $\hat{\mathcal{C}}$ to at most u .

This algorithm relies on the fact that no two distinct cycles in $\mathcal{C}^{(2L)}$ share more than one common column and row simultaneously. The minimality of $\hat{\mathcal{C}}$ is controlled by the parameter u .

The proposed algorithm is formally described in Algorithm 4. In the numerical experiments presented in a later section, we set $u = 2$. By leveraging the structure of UTCBCs, the estimation of \mathcal{C} can be performed with computational complexity that depends only on the constants J , L , and q , and is independent of P and the total number of physical qubits n .

Algorithm 4 Cycle Set Estimation Based on Recent Variable Node Changes

```

1:  $\hat{\mathcal{C}} \leftarrow \{\}$ 
2: for all  $j \in K_d^{(\ell)}$  do
3:   for all  $\mathcal{C} \in \mathcal{C}^{(2L)}$  such that  $j \in K(\mathcal{C})$  do
4:     if  $|K(\mathcal{C}) \cap K_d^{(\ell)}| \geq 2$  then
5:       add  $\mathcal{C}$  to  $\hat{\mathcal{C}}$ 
6:     if  $|\hat{\mathcal{C}}| > u$  then
7:       return null
8:     end if
9:     if  $K_d^{(\ell)} \subset K(\hat{\mathcal{C}})$  then
10:      return  $\hat{\mathcal{C}}$ 
11:    end if
12:  end if
13: end for
14: end for
15: return null

```

VI-G Proposed Post-Processing Decoder

In this section, we propose a post-processing decoding algorithm that supplements the noise estimation when the joint BP decoder stagnates after failing to find a noise estimate that satisfies the syndrome condition. Note that even if the estimate differs from the true noise $\underline{\xi} \neq \hat{\underline{\xi}}$, it may still be harmless for codeword recovery. Whether decoding is successful is determined by whether the condition $\underline{\xi} + \hat{\underline{\xi}} \in C_\Gamma^\perp$ is satisfied.

In the previous section, we identified a set of cycles $\hat{\mathcal{C}}$ from the estimated noise $\hat{\underline{\xi}}^{(\ell)}$ and its history. For brevity, we define $K := K(\hat{\mathcal{C}})$. Let $\bar{K} := [N] \setminus K$, and denote by $\hat{\underline{\xi}}_{\bar{K}}^{(\ell)}$ and $(H_\Delta)_{\bar{K}}$ the restriction of $\hat{\underline{\xi}}^{(\ell)}$ and H_Δ to the components indexed by \bar{K} , respectively. We have:

$$\underline{\sigma} = H_\Delta \underline{\xi} = (H_\Delta)_K \underline{\xi}_K + (H_\Delta)_{\bar{K}} \underline{\xi}_{\bar{K}} \quad (40)$$

Suppose the estimation $\hat{\mathcal{C}}$ is correct; that is, the joint BP algorithm is trapped in K , and the noise has been correctly estimated on the complement set \bar{K} , i.e., $K_{\text{err}}^{(\ell)} \subset K$. Equivalently, the following holds:

$$\hat{\underline{\xi}}_{\bar{K}}^{(\ell)} = \underline{\xi}_{\bar{K}}$$

Then, from (40), it follows that:

$$\underline{\sigma} = (H_\Delta)_K \underline{\xi}_K + (H_\Delta)_{\bar{K}} \hat{\underline{\xi}}_{\bar{K}}^{(\ell)} \quad (41)$$

Our proposed post-processing decoder solves this linear equation for $\underline{\xi}_K$, and assigns the solution as $\hat{\underline{\xi}}_K$. Together with $\hat{\underline{\xi}}_{\bar{K}} := \hat{\underline{\xi}}_{\bar{K}}^{(\ell)}$, this yields the final estimate $\hat{\underline{\xi}}$.

From Theorem 5, it is known that any cycle \mathcal{C} in the UTCBCs $\underline{u}(0)$ and $\underline{u}(1)$ does not contain any logical errors; that is, $N(\mathcal{C}; H_\Delta) \subset C_\Gamma^\perp$. As discussed in Discussion 1, the proposed code construction assigns the \mathbb{F}_q -valued entries so that any cycle in the UTCBC $\underline{u}(2)$ also avoids logical errors; specifically, $N(\mathcal{C}; H_\Delta) = \{0\}$. Therefore, if the set \mathcal{C} is correctly estimated, it follows that $\underline{\xi} + \hat{\underline{\xi}}$ must lie in C_Γ^\perp .

The total number of equations in (41) that involve any of the variables ξ_j for $j \in K$ is at most $|K|$. The size of K is upper bounded by $|K| \leq uL$, where u is the number of cycles in \mathcal{C} . In the experiments described later, we set $u = 2$.

Thus, the size of the resulting system of equations is quite small compared to the total number of physical qubits n . Both the algorithm for checking whether a solution exists and the algorithm for computing one such solution can be executed with computational complexity $O(|K|^3)$. Furthermore, the linear equation admits a solution, ensuring that the decoding success condition $\underline{\xi} + \hat{\underline{\xi}} \in C_{\Gamma}^{\perp}$ is satisfied.

Algorithm 5 outlines the complete decoding procedure, which combines joint BP decoding with the proposed post-processing step. The algorithm begins by running standard joint BP iterations. If a valid noise estimate satisfying the syndrome condition is found, the algorithm terminates and outputs the estimate. Otherwise, it continues iterating. If the decoder stagnates during the estimation of X-noise or Z-noise, the algorithm invokes a post-processing step. In this step, the decoder estimates a set of cycles $\hat{\mathcal{C}}$ responsible for trapping, and attempts to solve a linear system restricted to the support $K(\hat{\mathcal{C}})$. If a solution is found, it is assigned to the corresponding part of the noise estimate. The process continues until a valid estimate is obtained or the loop is manually terminated.

Algorithm 5 Joint Belief Propagation + Post-Processing Decoding Algorithm

```

1:  $\ell \leftarrow 0$ 
2: Initialize with the joint BP algorithm
3: while true do
4:    $\ell \leftarrow \ell + 1$ 
5:   Perform the  $\ell$ -th joint BP iteration
6:   if  $H_{\Delta}\hat{\underline{\xi}}^{(\ell)} = \underline{\sigma}$  and  $H_{\Gamma}\hat{\underline{\zeta}}^{(\ell)} = \underline{\tau}$  then
7:     Output the estimated noise  $(\hat{\underline{\xi}} := \hat{\underline{\xi}}^{(\ell)}, \hat{\underline{\zeta}} := \hat{\underline{\zeta}}^{(\ell)})$  and terminate
8:   end if
9:   if  $H_{\Gamma}\hat{\underline{\xi}}^{(\ell)} \neq \underline{\sigma}$  and joint BP algorithm stagnates in X-noise estimation then
10:    Determine  $\hat{\mathcal{C}}$  using the cycle-set estimation algorithm for  $H_{\Delta}$ 
11:    if  $\hat{\mathcal{C}} \neq \text{null}$  then
12:       $K := K(\hat{\mathcal{C}})$ 
13:      if  $\underline{\sigma} = (H_{\Delta})_K \underline{\xi}_K + (H_{\Delta})_{\overline{K}} \hat{\underline{\xi}}_K^{(\ell)}$  has a solution  $\underline{\xi}_K$  then
14:        Assign one such solution to  $\hat{\underline{\xi}}_K$  and  $\hat{\underline{\xi}}_{\overline{K}} := \hat{\underline{\xi}}_K^{(\ell)}$ 
15:      end if
16:    end if
17:  end if
18:  if  $H_{\Delta}\hat{\underline{\zeta}}^{(\ell)} \neq \underline{\tau}$  and joint BP algorithm stagnates in Z-noise estimation then
19:    Determine  $\hat{\mathcal{C}}$  using the cycle-set estimation algorithm for  $H_{\Gamma}$ 
20:    if  $\hat{\mathcal{C}} \neq \text{null}$  then
21:       $K := K(\hat{\mathcal{C}})$ 
22:      if  $\underline{\tau} = (H_{\Gamma})_K \underline{\zeta}_K + (H_{\Gamma})_{\overline{K}} \hat{\underline{\zeta}}_K^{(\ell)}$  has a solution  $\underline{\zeta}_K$  then
23:        Assign one such solution to  $\hat{\underline{\zeta}}_K$  and  $\hat{\underline{\zeta}}_{\overline{K}} := \hat{\underline{\zeta}}_K^{(\ell)}$ 
24:      end if
25:    end if
26:  end if
27:  if  $H_{\Delta}\hat{\underline{\xi}} = \underline{\sigma}$  and  $H_{\Gamma}\hat{\underline{\zeta}} = \underline{\tau}$  then
28:    Output the estimated noise  $(\hat{\underline{\xi}}, \hat{\underline{\zeta}})$  and terminate
29:  end if
30: end while

```

The proposed post-processing targets a cycle set \mathcal{C} composed of cycles of length $2L$. The next shortest cycles are those of length $2(L+2)$. These longer cycles may not be full-rank and could potentially contain logical errors. As will be discussed in the next section, when decoding the proposed codes with the proposed decoder, it is possible for the decoder to stagnate after becoming trapped in cycles of length $2(L+2)$. In such cases, one might consider adopting a decoding strategy that selects the most likely noise consistent with the syndrome. Such a strategy may, by chance, correctly match the true noise and succeed. However, it also risks resulting in an undetected decoding failure. To avoid this risk, the proposed decoder is designed to treat such cases as detectable decoding failures.

VII Results

This section presents the results of the proposed code construction and decoding method. We begin by describing the construction of the code matrices. We then evaluate the decoding performance of the proposed degeneracy-aware

decoder through numerical simulations over depolarizing channels. Finally, we analyze the minimum distance of the proposed code by enumerating short cycles in the Tanner graph.

VII-A Code Construction

Using Algorithm 1, we constructed APMs \underline{f} and \underline{g} , along with the corresponding matrices \hat{H}_X and \hat{H}_Z , for several choices of P , with fixed parameters $J = 2$ and $L = 6$. Although it would be preferable to select P as a power of two for implementation purposes, we found that doing so made it extremely difficult to simultaneously satisfy both conditions (a) and (b). Our experiments indicate that P must contain multiple small prime factors in order to admit valid sequences \underline{f} and \underline{g} . In particular, we were able to identify such sequences more easily when P was a multiple of $384 = 2^7 \cdot 3$, which represents a relatively simple composite case. The resulting pairs $(\underline{f}, \underline{g})$ of APMs are listed in Table II.

For the finite field construction, we set $e = 8$ and $q = 2^e$, and defined the field \mathbb{F}_q using the primitive polynomial $x^8 + x^4 + x^3 + x^2 + 1$ over \mathbb{F}_2 . Using Algorithm 2 and Algorithm 3, we constructed the matrices H_Γ and H_Δ . We used the instance with $P = 6500$, which was the largest value of P in Table II for which both Algorithm 2 and Algorithm 3 successfully completed. Specifically, the algorithms succeeded for $P = 2^i \cdot 3$ with $i = 7, 8, \dots, 11$, but failed for $P = 2^{12} \cdot 3$, where they were unable to generate H_Γ and H_Δ .

Each nonzero entry in H_Γ and H_Δ is then replaced by its corresponding $e \times e$ binary companion matrix (or its transpose), following the method described in Section VI-B, to obtain the binary matrices H_X and H_Z .

VII-B Numerical Simulation

We conducted numerical experiments over depolarizing channels with physical error rate p_D . The proposed decoding method was implemented using Algorithm 5, and decoding success or failure was determined using the degeneracy-aware criterion described in Section VI-A.

Figure 3 shows the decoding performance of the proposed code with $P = 6500$ using the degeneracy-aware decoder. The number of physical qubits is $n = eLP = 312000$. At a coding rate of $R = 1/3$ and physical error rate $p_D = 9.45\%$, the decoder achieves a frame error rate (FER) of 10^{-4} . This noise level is comparable to the threshold of surface codes, which operate at near-zero rates and typically cannot achieve this performance. Reaching FER = 10^{-4} at this noise level with $R = 1/3$ highlights the robustness of the proposed scheme. Moreover, the decoding complexity scales linearly with the number of physical qubits n .

For comparison, we also plot the decoding performance of a code constructed using the method of [31] with the same parameters (P, q, J, L) . The conventional decoding method corresponds to joint BP decoding without any post-processing.

The proposed method exhibits a slightly inferior performance in the waterfall region compared to the conventional one. This behavior is consistent with a well-known phenomenon in LDPC code design: algebraically constructed LDPC codes, which are designed to achieve large girth and minimum distance, tend to exhibit better performance in the error floor region but may perform worse in the waterfall region [41]. Conversely, randomly constructed LDPC codes generally perform well in the waterfall region, but they often suffer from higher error floors.

The strategy discussed in the previous section functioned as intended: all decoding failures were detectable. That is, there were no cases in which the estimated noise $\hat{\xi}$ satisfied $H_\Delta \hat{\xi} = \sigma$ while $\hat{\xi}$ belonged to $C_\Delta \setminus C_\Gamma^\perp$. All observed decoding failures in the error floor region were caused by errors trapped in cycles of length $2(L + 2)$. Once such a structure was detected, the decoder was configured to declare a decoding failure.

VII-C Computing Upper Bound of Minimum Distance

For the proposed code (C_X, C_Z) , we evaluate an upper bound on the minimum distance in this section. It is known that, for binary LDPC codes with column weight 2, all codewords can be constructed from the union of cycles [42]. This also holds for nonbinary LDPC codes.

Our approach for computing an upper bound on the minimum distance d_X is as follows. The same procedure is applied to compute an upper bound on d_Z .

- 1) First, we enumerate short Tanner cycles \mathcal{C} in H_Γ .
- 2) Next, for each cycle \mathcal{C} , we enumerate nonzero codewords $\underline{\xi} \in N(\mathcal{C}; H_\Gamma)$ that are not contained in C_Δ^\perp .
- 3) Among all such codewords, we take the smallest bitwise Hamming weight as an upper bound on d_X .

Both C_X and C_Z are designed to have girth 12. That is, cycles of length 12 are the shortest cycles in the Tanner graphs of the codes. For any cycle \mathcal{C} of length 12, we have constructed the code such that the corresponding subcode $N(\mathcal{C}; H_\Gamma)$ is either contained in C_Δ^\perp or has dimension zero. Hence, such cycles do not contribute to the minimum distance d_X of C_X (see (12)). The same holds for d_Z of C_Z .

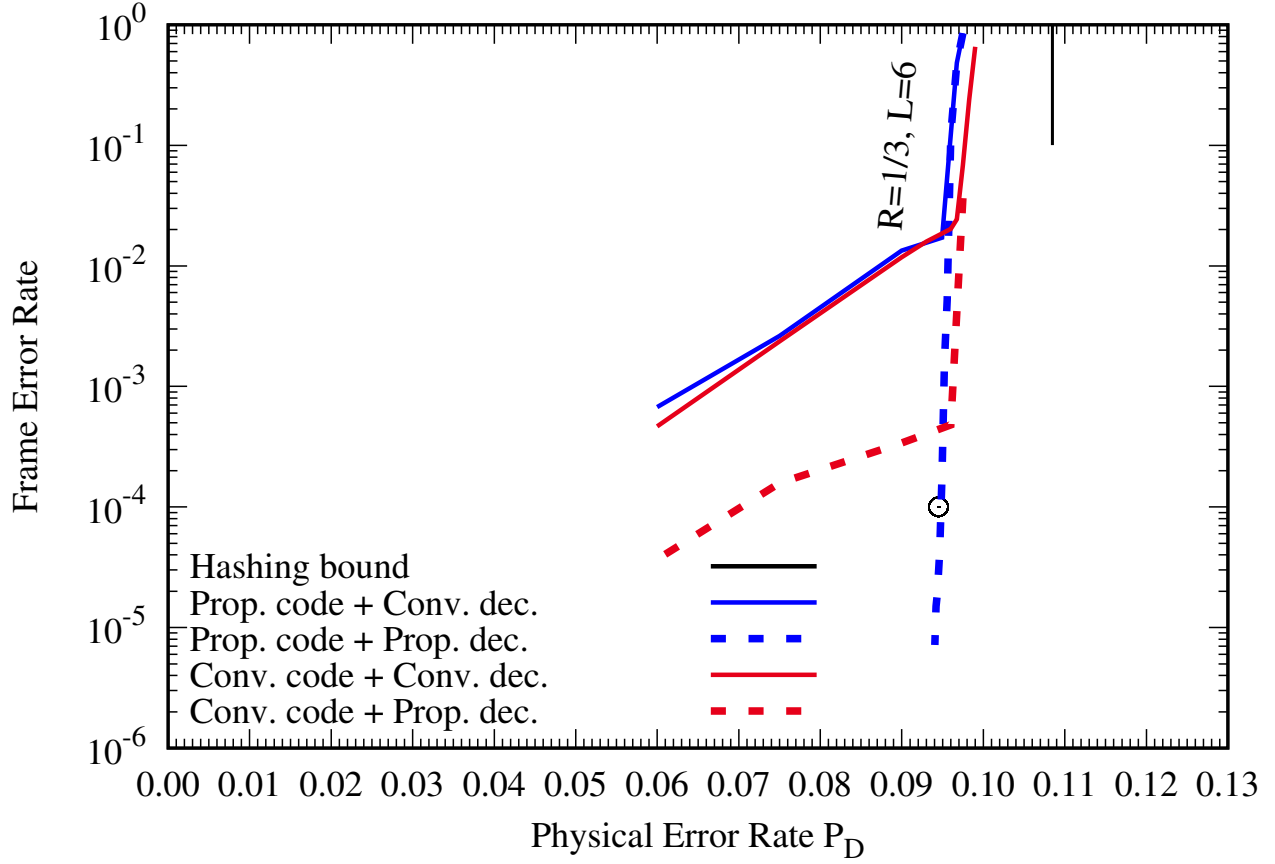


Fig. 3: Comparison of decoding performance between the proposed $[[312000, 104000, \leq 14]]$ code and the conventional $[[312000, 104000, \leq 10]]$ code [31], both having the same code length and rate $R = 1/3$. The proposed code reaches $\text{FER} = 10^{-4}$ at $p_D = 9.45\%$, a noise level typically unachievable by conventional codes with such high rate, highlighting the effectiveness of our construction in pushing the performance toward the hashing bound.

We now consider the next shortest cycles, those of length 16. We first enumerated all length-16 cycles C in the Tanner graph of C_X . For each cycle, we computed the determinant of the corresponding submatrix. This determinant is either L or $L - 1$. In the former case, the subcode $N(C; H_\Gamma) \subset C_\Gamma$ contains only the zero vector; in the latter case, it contains $q - 1$ nonzero codewords. We take the minimum bitwise Hamming weight among these nonzero codewords as an upper bound on d_Z . An upper bound on d_Z of C_Z is computed in the same manner.

Using this approach, we evaluated an upper bound on the minimum distance of the proposed code. In total, we identified 1402 and 1396 length-16 cycles whose determinant is $L - 1$ in H_Γ and H_Δ , respectively. By computing the bitwise weights of the corresponding codewords-excluding those that lie in C_Δ^\perp and C_Γ^\perp , respectively-we obtained the weight distributions $A_X(w)$ and $A_Z(w)$, as shown in Table IV.

For comparison, we also computed $A_X(w)$ and $A_Z(w)$ for the conventional codes used in Section VII-B. In the conventional code, there exist length-12 cycles C in the UTCBC $\underline{u}(2)$ in H_Γ such that $N(C; H_\Gamma)$ contains nonzero codewords that are not included in C_Δ^\perp . These codewords were enumerated and included in the weight distribution $A_X(w)$. The distribution $A_Z(w)$ was computed in the same manner.

In Table IV, we list the weight distributions of the proposed and conventional codes. The upper bounds on the minimum bitwise distance are 14 and 10 for the proposed and conventional codes, respectively. The conventional code contains many low-weight codewords, which are likely responsible for the observed error floor. In contrast, the proposed code includes fewer low-weight codewords arising from short cycles, which we believe is the key reason why it avoids the error floor.

We note that the minimum bitwise weight observed among the enumerated length-16 cycles is 14. While this value provides an upper bound on the minimum distance, it may not be exact: it is possible that codewords arising from longer cycles or from combinations of cycles in the Tanner graph have lower bitwise Hamming weights, despite having \mathbb{F}_q weights of at least 10. Nonetheless, due to the use of a relatively large field size q , we believe that the bound is likely to be tight.

TABLE IV: Weight distribution of codewords formed from the short cycles. Here, $A_X(w)$ and $A_Z(w)$ denote the number of codewords of weight w in $C_X \setminus C_Z^\perp$ and $C_Z \setminus C_X^\perp$, respectively.

w	Prop.		Conv.	
	$A_X(w)$	$A_Z(w)$	$A_X(w)$	$A_Z(w)$
10	0	0	2	4
11	0	0	8	4
12	0	0	35	33
13	0	0	109	91
14	0	2	257	262
15	0	6	593	647
16	4	9	1255	1354
17	9	12	2674	2520
18	33	46	4751	4747
19	111	114	7530	7721
20	266	274	11363	11249
21	643	611	15059	15276
22	1277	1276	18985	18985
23	2509	2360	21517	21733
24	4394	4154	22499	22916
25	7350	7245	21497	21693
26	10952	11102	19119	19543
27	15725	15624	15532	15993
28	21109	21190	12019	11757
29	26060	26526	8061	8259
30	31305	30931	5246	5156
31	34721	34512	2989	2941
32	36401	35851	1614	1642
33	35065	34931	793	746
34	32146	32092	346	344
35	27484	27441	132	152
36	22073	22069	45	49
37	16718	16730	15	14
38	11865	11859	6	7
39	8108	7856	3	1
40	4962	5071	1	1
41	2926	2919	0	0
42	1667	1666	0	0
43	898	821	0	0
44	412	393	0	0
45	199	181	0	0
46	73	64	0	0
47	28	26	0	0
48	9	9	0	0
49	6	5	0	0
50	2	2	0	0
total	255×1402	255×1396	255×761	255×768

VIII Conclusion and Future Work

In this paper, we proposed a construction and decoding method for quantum error correction using non-binary LDPC codes, with a focus on explicitly exploiting degeneracy. We introduced key design criteria to control cycle structure in the parity-check matrices and developed a degeneracy-aware post-processing decoder to address decoding stagnation.

Our construction utilizes APMs to ensure algebraic structure while maintaining randomness through selective sampling. This decoder dynamically estimates the subset of cycles responsible for the stagnation and corrects errors via constrained linear solving.

Simulation results demonstrated that our code achieves FER of 10^{-4} at a physical error rate of 9.45% for rate-1/3 codes, achieving performance comparable to that of surface codes in the error floor regime while maintaining higher coding rates. Furthermore, upper bounds on the minimum distance derived from cycle enumeration confirmed the structural advantages of the proposed code over conventional constructions. Importantly, the decoding complexity scales linearly with the number of physical qubits, making the proposed method suitable for large-scale implementation.

Future work includes extending the proposed framework to support lower-rate quantum LDPC codes and exploring the feasibility of applying the proposed degeneracy-aware decoding strategy to binary LDPC codes. These directions may further broaden the applicability of our approach and enable practical deployment in systems where qubit and complexity constraints are stringent.

Acknowledgment

This study was carried out using the TSUBAME4.0 supercomputer at Institute of Science Tokyo.

Appendix A Companion Matrix Representation over Finite Fields

This section introduces the companion matrix representation of finite field elements over \mathbb{F}_{2^e} . We begin by reviewing the vector representation of field elements via the mapping \underline{v} , and then define the companion matrix $A(\alpha)$ associated with a primitive element α . The main result is that multiplication in \mathbb{F}_{2^e} can be translated into matrix-vector multiplication over \mathbb{F}_2 , providing a linear-algebraic framework that is crucial for decoding operations in quantum LDPC codes. Several theorems are presented to formalize the algebraic properties of these representations, including linearity, multiplicativity, and the equivalence between field equations and their matrix representations.

Let $q = 2^e$. It is well-known that elements of the finite field \mathbb{F}_q can be commonly represented either as binary vectors of length e or as polynomials of degree less than e with binary coefficients. Let $\alpha \in \mathbb{F}_q$ be a primitive element. Any element $\gamma \in \mathbb{F}_q$ can be uniquely written in the form

$$\gamma = \sum_{j=0}^{e-1} g_j \alpha^j.$$

We define the mapping $\underline{v} : \mathbb{F}_q \rightarrow \mathbb{F}_2^e$ by

$$\underline{v}(\gamma) := (g_0, g_1, \dots, g_{e-1})^\top \in \mathbb{F}_2^e.$$

Example 9. For $e = 8$, using the primitive polynomial $x^8 + x^4 + x^3 + x^2 + 1$ over \mathbb{F}_2 , we have:

$$\begin{aligned} \underline{v}(0) &= (00000000)^\top, \\ \underline{v}(1) &= (10000000)^\top, \\ \underline{v}(\alpha) &= (01000000)^\top, \\ \underline{v}(\alpha^{e-1}) &= (00000001)^\top, \\ \underline{v}(\alpha^e) &= (10110000)^\top, \end{aligned}$$

□

Theorem 6. The map \underline{v} defines an isomorphism of vector spaces over \mathbb{F}_2 , and also a group isomorphism under addition:

$$\underline{v}(\gamma_1 + \gamma_2) = \underline{v}(\gamma_1) + \underline{v}(\gamma_2), \quad \forall \gamma_1, \gamma_2 \in \mathbb{F}_q.$$

Proof. Let $\gamma_1, \gamma_2 \in \mathbb{F}_q$. Since $\mathbb{F}_q = \mathbb{F}_{2^e}$ is an \mathbb{F}_2 -vector space with basis $\{1, \alpha, \dots, \alpha^{e-1}\}$, each γ_i has a unique representation

$$\gamma_1 = \sum_{j=0}^{e-1} g_j^{(1)} \alpha^j, \quad \gamma_2 = \sum_{j=0}^{e-1} g_j^{(2)} \alpha^j \quad (g_j^{(i)} \in \mathbb{F}_2).$$

Thus,

$$\gamma_1 + \gamma_2 = \sum_{j=0}^{e-1} (g_j^{(1)} + g_j^{(2)}) \alpha^j.$$

Hence,

$$\underline{v}(\gamma_1 + \gamma_2) = (g_0^{(1)} + g_0^{(2)}, \dots, g_{e-1}^{(1)} + g_{e-1}^{(2)})^\top = \underline{v}(\gamma_1) + \underline{v}(\gamma_2).$$

Therefore, \underline{v} is a homomorphism with respect to addition, and it is a linear isomorphism over \mathbb{F}_2 , as it extracts coefficients from a linear combination and both \mathbb{F}_q and \mathbb{F}_2^e have the same dimension. □

They can also be naturally represented using $e \times e$ binary matrices.

Definition 2. Let $a(x) = a_0 + a_1 x + \dots + a_e x^e$ with $a_0 = a_e = 1$ be the primitive polynomial of $\alpha \in \mathbb{F}_q$. The *companion matrix* $A(\alpha)$ [43] is defined as:

$$\begin{aligned} A(\alpha) &\stackrel{\text{def}}{=} (\underline{v}(\alpha^1), \underline{v}(\alpha^2), \dots, \underline{v}(\alpha^e)) \\ &= \begin{pmatrix} 0 & 0 & 0 & 0 & a_0 \\ 1 & 0 & 0 & 0 & a_1 \\ 0 & 1 & 0 & 0 & a_2 \\ \vdots & \vdots & \ddots & \vdots & \vdots \\ 0 & 0 & 0 & 1 & a_{e-1} \end{pmatrix}. \end{aligned}$$

We define the mapping $A : \mathbb{F}_q \rightarrow \mathbb{F}_2^{e \times e}$ by

$$\begin{aligned} A(0) &\stackrel{\text{def}}{=} O, \\ A(\alpha^l) &\stackrel{\text{def}}{=} A(\alpha)^l, \quad \text{for } l = 0, \dots, q-2. \end{aligned}$$

□

The mapping $A : \mathbb{F}_q \rightarrow \mathbb{F}_2^{e \times e}$ introduced above has important algebraic properties. Specifically, it preserves the algebraic structure of the finite field \mathbb{F}_q , as demonstrated in the following theorem.

Theorem 7. As shown in [43], the map A is injective, and its image $A(\mathbb{F}_q)$ forms a field isomorphic to \mathbb{F}_q . The map satisfies the following properties for all $\gamma_1, \gamma_2, \delta \in \mathbb{F}_q$: multiplicativity, commutativity, and additivity:

$$\begin{aligned} A(\gamma_1\gamma_2) &= A(\gamma_1)A(\gamma_2) = A(\gamma_2)A(\gamma_1), \\ A(\gamma)\underline{v}(\delta) &= \underline{v}(\gamma\delta), \end{aligned} \tag{42}$$

$$A(\gamma_1 + \gamma_2) = A(\gamma_1) + A(\gamma_2). \tag{43}$$

Proof. The case for the zero element is trivial, so we assume that $\gamma_1, \gamma_2, \delta \in \mathbb{F}_q^\times$. Let $\underline{e}^{(i)}$ denote the standard basis vector of \mathbb{F}_2^e whose i th component is 1 and the others are 0. By the definition of \underline{v} , we have $\underline{v}(\alpha^i) = \underline{e}^{(i)}$. Furthermore, by the definition of the companion matrix $A(\alpha)$, its action on $\underline{e}^{(i)}$ corresponds to the i th column of $A(\alpha)$. Hence, we have

$$A(\alpha)\underline{v}(\alpha^i) = \underline{v}(\alpha^{i+1}) \quad \text{for all } i \in [e]. \tag{44}$$

Let $\gamma_1 = \alpha^i$ and $\gamma_2 = \alpha^j$. Then, since $A(\alpha^k) = A(\alpha)^k$ for all $k \in \mathbb{Z}$, we have

$$A(\gamma_1)A(\gamma_2) = A(\alpha^i)A(\alpha^j) = A(\alpha)^{i+j} = A(\alpha^{i+j}) = A(\gamma_1\gamma_2),$$

which establishes both multiplicativity and commutativity. To prove (42), suppose $\gamma = \alpha^j$ and $\delta = \alpha^i$. Then,

$$A(\gamma)\underline{v}(\delta) = A(\alpha^j)\underline{v}(\alpha^i) = A(\alpha)^j\underline{v}(\alpha^i) = \underline{v}(\alpha^{i+j}) = \underline{v}(\gamma\delta),$$

where we used (44) repeatedly. To prove (43), note that for any $\delta \in \mathbb{F}_q$, we compute:

$$(A(\gamma_1) + A(\gamma_2))\underline{v}(\delta) = A(\gamma_1)\underline{v}(\delta) + A(\gamma_2)\underline{v}(\delta) = \underline{v}(\gamma_1\delta) + \underline{v}(\gamma_2\delta) = \underline{v}((\gamma_1 + \gamma_2)\delta) = A(\gamma_1 + \gamma_2)\underline{v}(\delta).$$

Since \underline{v} is injective, the equality

$$A(\gamma_1 + \gamma_2) = A(\gamma_1) + A(\gamma_2)$$

follows. □

The matrix representation $A(\gamma)$ not only captures the algebraic operations in \mathbb{F}_q , but also provides a useful tool for performing field multiplication and addition in terms of binary vector and matrix operations. In particular, the mapping A allows us to translate scalar equations over \mathbb{F}_q into linear-algebraic expressions over \mathbb{F}_2 via the map \underline{v} .

The following theorem illustrates a basic but important connection between the vector representation $\underline{v}(\alpha^i)$ and the matrix representation $A(\alpha^i)$.

Theorem 8. The vector $\underline{v}(\alpha^i)$ agrees with the leftmost column of $A(\alpha^i)$.

Proof. From the multiplication property,

$$A(\gamma_1)\underline{v}(\gamma_2) = \underline{v}(\gamma_1\gamma_2).$$

Let $\gamma_1 = \alpha^i$ and $\gamma_2 = 1 = \alpha^0$. Then

$$A(\alpha^i)\underline{v}(1) = \underline{v}(\alpha^i).$$

Since $\underline{v}(1) = (1, 0, \dots, 0)^\top$, this implies that $\underline{v}(\alpha^i)$ agrees with the first column of $A(\alpha^i)$, which completes the proof. □

The next theorem provides an equivalence between scalar linear combinations over \mathbb{F}_q and their binary vector representations using matrix multiplication. This property will be useful when solving equations or decoding in vectorized form.

Theorem 9. The following equivalence holds for any $\delta_j, \xi_j, \sigma \in \mathbb{F}_q$:

$$\sum_j \delta_j \xi_j = \sigma \quad \text{if and only if} \quad \sum_j A(\delta_j) \underline{v}(\xi_j) = \underline{v}(\sigma).$$

Proof. Using the additivity of \underline{v} and the multiplicative property $A(\gamma)\underline{v}(\delta) = \underline{v}(\gamma\delta)$ from (42), we compute:

$$\begin{aligned}\sum_j A(\delta_j) \underline{v}(\xi_j) &= \sum_j \underline{v}(\delta_j \xi_j) \\ &= \underline{v}\left(\sum_j \delta_j \xi_j\right).\end{aligned}$$

Therefore, the identity $\sum_j A(\delta_j) \underline{v}(\xi_j) = \underline{v}(\sigma)$ holds if and only if $\underline{v}\left(\sum_j \delta_j \xi_j\right) = \underline{v}(\sigma)$. Since \underline{v} is injective, this is equivalent to $\sum_j \delta_j \xi_j = \sigma$. \square

Appendix B Finite Field Generated by $A(\alpha)^T$

In the previous section, we studied the algebraic structure of the field generated by the companion matrix $A(\alpha)$, which faithfully represents multiplication in \mathbb{F}_q . In this section, we turn our attention to the transpose matrix $A(\alpha)^T$, which also generates a field isomorphic to \mathbb{F}_q .

Our goal is to examine the algebraic properties of this transposed field representation and to define a new binary mapping $\underline{w}(\cdot)$ that works analogously with $A(\cdot)^T$, in a manner similar to $\underline{v}(\cdot)$ and $A(\cdot)$ discussed previously. This will be important, for example, in dual code constructions or applications where right multiplication by vectors is preferable. Specifically, we aim to identify the corresponding map $\underline{w}(\cdot)$ that yields similar algebraic properties when used in conjunction with $A(\cdot)^T$, analogous to those established in Theorem 7.

Definition 3. Define the mapping $A^T : \mathbb{F}_q \rightarrow \mathbb{F}_2^{e \times e}$ as follows:

$$\begin{aligned}A^T(0) &\stackrel{\text{def}}{=} O, \\ A^T(\alpha^i) &\stackrel{\text{def}}{=} (A(\alpha)^T)^i = (A(\alpha)^i)^T \quad \text{for } i = 0, \dots, q-2.\end{aligned}$$

\square

The matrix mapping $A^T(\cdot)$ inherits many of the algebraic properties of $A(\cdot)$, thanks to the fact that transposition preserves both addition and multiplication of matrices when defined over a field. In particular, since $A(\alpha)$ generates a field isomorphic to \mathbb{F}_q , its transpose $A(\alpha)^T$ does as well. The following theorem summarizes the basic algebraic structure of the set $A^T(\mathbb{F}_q)$, and shows that it forms a field isomorphic to \mathbb{F}_q . This will be particularly useful when we consider right-multiplication by row vectors in the next section.

Theorem 10. The map A^T is injective, and its image $A^T(\mathbb{F}_q) \subset \mathbb{F}_2^{e \times e}$ forms a field that is isomorphic to \mathbb{F}_q under the correspondence defined by A^T . The following properties hold for all $\gamma_1, \gamma_2 \in \mathbb{F}_q$:

$$A^T(\gamma_1 + \gamma_2) = A^T(\gamma_1) + A^T(\gamma_2), \tag{45}$$

$$A^T(\gamma_1 \gamma_2) = A^T(\gamma_1) A^T(\gamma_2). \tag{46}$$

Proof. Since $A^T(\gamma)$ is the transpose of $A(\gamma)$, the result follows immediately from Theorem 7. \square

We define $\underline{w}(0) \stackrel{\text{def}}{=} (0, \dots, 0) \in \mathbb{F}_2^e$. For $i = 1, \dots, q-1$, define $\underline{w}(\alpha^i) \in \mathbb{F}_2^e$ as the first column of $A^T(\alpha^i)$. Note that this definition is analogous to the map $\underline{v} : \mathbb{F}_q \rightarrow \mathbb{F}_2^e$ introduced in the previous section, where $\underline{v}(\alpha^i)$ corresponds to the i th standard basis vector and satisfies $A(\gamma)\underline{v}(\delta) = \underline{v}(\gamma\delta)$.

In contrast, as we will prove in Theorem 11, the map $\underline{w}(\cdot)$ satisfies the relation

$$A^T(\gamma)\underline{w}(\delta) = \underline{w}(\gamma\delta),$$

which mirrors the behavior of $\underline{v}(\cdot)$, but with respect to the transpose operator. In particular, while $\underline{v}(\gamma)$ is obtained as a column of $A(\gamma)$, $\underline{w}(\gamma)$ is constructed from the row structure of $A(\gamma)$ via transposition.

This symmetry between \underline{v} and \underline{w} allows us to characterize linear relations and matrix actions in terms of either map, depending on whether we prefer right or left multiplication.

The map $\underline{w} : \mathbb{F}_q \rightarrow \mathbb{F}_2^e$, defined as the first column of $A^T(\gamma)$, also preserves addition. That is, for all $\gamma_1, \gamma_2 \in \mathbb{F}_q$, we have

$$\underline{w}(\gamma_1 + \gamma_2) = \underline{w}(\gamma_1) + \underline{w}(\gamma_2),$$

which follows directly from the additivity of $A^T(\cdot)$ given in (45). Therefore, \underline{w} defines a group isomorphism between $(\mathbb{F}_q, +)$ and $(\mathbb{F}_2^e, +)$.

Theorem 11. The following multiplicative property holds for all $\gamma_1, \gamma_2 \in \mathbb{F}_q$:

$$A^T(\gamma_1) \underline{w}(\gamma_2) = \underline{w}(\gamma_1 \gamma_2).$$

Proof. If either γ_1 or γ_2 is zero, both sides are clearly zero, so the identity holds trivially. Suppose now that $\gamma_1 = \alpha^j$ and $\gamma_2 = \alpha^i$ for some $i, j \in \mathbb{Z}_{\geq 0}$.

By the definition of $\underline{w}(\cdot)$, we have

$$\underline{w}(\alpha^i) = A^T(\alpha^i) e^{(0)} = A^T(\alpha^i) \underline{w}(\alpha^0) = A^T(\alpha^i) \underline{w}(1). \quad (47)$$

Using the multiplicativity of $A^T(\cdot)$ established in (46), we have:

$$\begin{aligned} A^T(\alpha^j) \underline{w}(\alpha^i) &\stackrel{(47)}{=} A^T(\alpha^j) A^T(\alpha^i) \underline{w}(1) \\ &= A^T(\alpha^{i+j}) \underline{w}(1) \\ &\stackrel{(47)}{=} \underline{w}(\alpha^{i+j}), \end{aligned}$$

where all exponents are interpreted modulo $q - 1$. Hence, the identity holds for all $\gamma_1, \gamma_2 \in \mathbb{F}_q^\times$, and the general case follows. \square

To facilitate the expression of scalar relations over \mathbb{F}_q in terms of binary matrix operations involving $A^T(\cdot)$, we introduce the mapping $\underline{w} : \mathbb{F}_q \rightarrow \mathbb{F}_2^e$, which plays a role analogous to $\underline{v}(\cdot)$ used with $A(\cdot)$. In particular, $\underline{w}(\cdot)$ is designed to interact naturally with the transposed field representation so that right-multiplication corresponds to field multiplication. The following theorem establishes the fundamental equivalence between scalar linear combinations over \mathbb{F}_q and their binary vector representation via $A^T(\cdot)$ and $\underline{w}(\cdot)$.

Theorem 12. The following equivalence holds for any $\gamma_j, \delta_j, \tau \in \mathbb{F}_q$:

$$\sum_j \gamma_j \zeta_j = \tau \iff \sum_j A^T(\gamma_j) \underline{w}(\zeta_j) = \underline{w}(\tau).$$

Proof. This can be shown by an argument analogous to that of Theorem 9. Using the multiplicativity of $A^T(\cdot)$, we have $A^T(\gamma_j) \underline{w}(\zeta_j) = \underline{w}(\gamma_j \zeta_j)$. Therefore,

$$\sum_j A^T(\gamma_j) \underline{w}(\zeta_j) = \sum_j \underline{w}(\gamma_j \zeta_j) = \underline{w}\left(\sum_j \gamma_j \zeta_j\right).$$

Thus, the left-hand side equals $\underline{w}(\tau)$ if and only if $\sum_j \gamma_j \zeta_j = \tau$, since \underline{w} is injective. \square

TABLE V: Companion matrices and binary representation for primitive element $\alpha \in \mathbb{F}_8$ with primitive polynomial $a(x) = 1 + x + x^3$.

i	0	1	2	3	4	5	6
α^i	α^0	α^1	α^2	α^3	α^4	α^5	α^6
$\underline{w}(\alpha^i)$	$(100)^T$	$(010)^T$	$(001)^T$	$(110)^T$	$(011)^T$	$(111)^T$	$(101)^T$
A^i	$\begin{pmatrix} 100 \\ 010 \\ 001 \end{pmatrix}$	$\begin{pmatrix} 001 \\ 101 \\ 010 \end{pmatrix}$	$\begin{pmatrix} 010 \\ 011 \\ 101 \end{pmatrix}$	$\begin{pmatrix} 101 \\ 111 \\ 011 \end{pmatrix}$	$\begin{pmatrix} 011 \\ 110 \\ 111 \end{pmatrix}$	$\begin{pmatrix} 111 \\ 100 \\ 110 \end{pmatrix}$	$\begin{pmatrix} 110 \\ 001 \\ 100 \end{pmatrix}$
$\underline{w}(\alpha^i)$	$(100)^T$	$(001)^T$	$(010)^T$	$(101)^T$	$(011)^T$	$(111)^T$	$(110)^T$
$(A^T)^i$	$\begin{pmatrix} 100 \\ 010 \\ 001 \end{pmatrix}$	$\begin{pmatrix} 010 \\ 001 \\ 110 \end{pmatrix}$	$\begin{pmatrix} 001 \\ 110 \\ 011 \end{pmatrix}$	$\begin{pmatrix} 110 \\ 011 \\ 111 \end{pmatrix}$	$\begin{pmatrix} 011 \\ 111 \\ 101 \end{pmatrix}$	$\begin{pmatrix} 111 \\ 101 \\ 100 \end{pmatrix}$	$\begin{pmatrix} 101 \\ 100 \\ 010 \end{pmatrix}$

Appendix C

Proof for (11)

The orthogonality of H_X and H_Z follows from the linearity and multiplicativity of the companion matrix mapping A , together with the orthogonality of the underlying non-binary matrices H_Γ and H_Δ :

$$\begin{aligned} (H_X H_Z^\top)_{i,j} &= \sum_k A(\gamma_{i,k}) A(\delta_{k,j}) \\ &= \sum_k A(\gamma_{i,k} \delta_{k,j}) \\ &= A\left(\sum_k \gamma_{i,k} \delta_{k,j}\right) \\ &= A((H_\Gamma H_\Delta^\top)_{i,j}) \\ &= A(0) \\ &= O. \end{aligned}$$

Appendix D

Proof for (9) and (10)

In this appendix, we show that if the orthogonality condition (7):

$$H_\Gamma(H_\Delta)^\top = O$$

holds, then the congruence relations (9) and (10):

$$\begin{pmatrix} -\hat{H}_Z^{(L)} & | & \hat{H}_Z^{(R)} & | & \hat{H}_Z^{(L)} & | & -\hat{H}_Z^{(R)} \end{pmatrix} \log \underline{\gamma} = \underline{0} \pmod{q-1},$$

$$\begin{pmatrix} -\hat{H}_X^{(L)} & | & \hat{H}_X^{(R)} & | & \hat{H}_X^{(L)} & | & -\hat{H}_X^{(R)} \end{pmatrix} \log \underline{\delta} = \underline{0} \pmod{q-1}$$

necessarily follow.

Let $\underline{\delta}_{jr}^\top$ denote the r -th row of $H_\Delta^{(j)}$, where $H_\Delta^{(j)}$ is the j -th row block of H_Δ . By the orthogonality condition, we have $H_\Gamma \underline{\delta}_{jr} = \underline{0}$. Note that H_Γ shares the same support (i.e., positions of nonzero entries) as \hat{H}_X , which is structured in a specific pattern. According to Theorem 4, the submatrix of $H_\Gamma h_{jr}$ that contributes to this equation forms a square matrix of size L , and it constitutes a Tanner cycle \mathcal{C} contained in the UTCBC $u(j)$ (defined in Section IV-A) in H_Γ .

As shown in the proof of Theorem 4, the Tanner cycle \mathcal{C} starts from the $(0, 0)$ block and traverses four elements in a clockwise direction, repeating this pattern for $L/2$ rounds. Label the elements visited in the order of the cycle as follows:

$$\begin{aligned} \gamma_0^{(0)} &\rightarrow \gamma_1^{(0)} \rightarrow \gamma_2^{(0)} \rightarrow \gamma_3^{(0)} \rightarrow \\ \gamma_0^{(1)} &\rightarrow \gamma_1^{(1)} \rightarrow \gamma_2^{(1)} \rightarrow \gamma_3^{(1)} \rightarrow \\ &\vdots \\ \gamma_0^{(L/2-1)} &\rightarrow \gamma_1^{(L/2-1)} \rightarrow \gamma_2^{(L/2-1)} \rightarrow \gamma_3^{(L/2-1)} \rightarrow \gamma_0^{(0)}. \end{aligned} \tag{48}$$

Note that for each $\ell \in [L/2]$, the elements $\gamma_1^{(\ell)}$ and $\gamma_2^{(\ell)}$ lie in the same column in the right half of H_Γ , while $\gamma_3^{(\ell)}$ and $\gamma_0^{(\ell+1)}$ lie in the same column in the left half of H_Γ . The set of all such columns coincides with the support (i.e., nonzero positions) of $\underline{\delta}_{jr}$.

The determinant of this submatrix \mathcal{C} is given by

$$\prod_{\ell \in [L/2]} \gamma_0^{(\ell)} \gamma_2^{(\ell)} + \prod_{\ell \in [L/2]} \gamma_1^{(\ell)} \gamma_3^{(\ell)}. \tag{49}$$

Since we work over a finite field of characteristic 2, i.e., $q = 2^e$, the sign does not affect the result. Since we work over a finite field of characteristic 2, i.e., $q = 2^e$, the sign does not affect the result. Moreover, since \mathcal{C} is orthogonal to the vector extracted from the nonzero entries of $\underline{\delta}_{jr}$, the rank of \mathcal{C} must be deficient, that is, strictly less than L , and hence (49) must equal zero. Therefore, the following equation holds:

$$\prod_{\ell \in [L/2]} \frac{\gamma_1^{(\ell)} \gamma_3^{(\ell)}}{\gamma_0^{(\ell)} \gamma_2^{(\ell)}} = 1.$$

Applying the discrete logarithm $\log_\alpha(\cdot)$ (with the base α omitted), we obtain

$$\sum_{\ell \in [L/2]} (-\log \gamma_0^{(\ell)} + \log \gamma_1^{(\ell)} + \log \gamma_3^{(\ell)} - \log \gamma_2^{(\ell)}) = 0 \pmod{q-1}. \quad (50)$$

Observe that the columns in which the variables $\gamma_i^{(\ell)}$ for $\ell \in [L/2]$ appear in H_Γ coincide with the positions of nonzero entries in the r -th row of the j -th row block of $\hat{H}_Z^{(L)}$. The same holds for $\gamma_3^{(\ell)}$. Likewise, the variables $\gamma_i^{(\ell)}$ for $i = 1, 2$ appear in the same columns as the nonzero entries in the r -th row of the j -th row block of $\hat{H}_Z^{(R)}$.

Let \underline{h}_{jr}^\top denote the r -th row in the j -th row block of \hat{H}_X . We write the left and right halves of \underline{h}_{jr}^\top as $\underline{h}_{jr,L}^\top$ and $\underline{h}_{jr,R}^\top$, respectively. Recall the definition of $\underline{\gamma} = (\gamma_0, \dots, \gamma_{2N-1})$ given in (8). The first and second halves of the vector $\underline{\gamma}$ correspond to the N symbols γ_{ij} that appear in the upper and lower rows of H_Γ , respectively, arranged from left to right. Recall that for each $\ell \in [L/2]$, the elements $\gamma_1^{(\ell)}$ and $\gamma_2^{(\ell)}$ lie in the same column in the right half of H_Γ , while $\gamma_3^{(\ell)}$ and $\gamma_0^{(\ell+1)}$ lie in the same column in the left half of H_Γ . Based on this structure, equation (50) can be rewritten as follows.

$$\left(\begin{array}{c|c|c|c} -\underline{h}_{jr,L}^\top & \underline{h}_{jr,R}^\top & \underline{h}_{jr,L}^\top & -\underline{h}_{jr,R}^\top \end{array} \right) \log \underline{\gamma} = \underline{0} \pmod{q-1}.$$

Since this argument applies to all $j \in [J]$ and $r \in [P]$, we can represent it in matrix-vector form as:

$$\left(\begin{array}{c|c|c|c} -\hat{H}_Z^{(L)} & \hat{H}_Z^{(R)} & \hat{H}_Z^{(L)} & -\hat{H}_Z^{(R)} \end{array} \right) \log \underline{\gamma} = \underline{0} \pmod{q-1}.$$

This establishes (9). The identity (10) can be proved in the same manner.

Appendix E Proof of (21) and (22)

In this section, we prove that Equation (21) is equivalent to the condition that every Tanner cycle \mathbf{C} contained in the UTCBC $\underline{u}(2)$ in H_Γ satisfies that $N(\mathbf{C}; H_\Gamma)$ contains no nonzero codewords.

Let \mathbf{C} be a Tanner cycle of length $2L$ included in the UTCBC $\underline{u}(2)$, which intersects the r -th row of $H_\Delta^{(2)}$. Note that \hat{H}_Z shares the same support (i.e., positions of nonzero entries) as H_Δ . Following the discussion in Appendix D, we label each variable in \mathbf{C} as in Equation (48). The dimension of $N(\mathbf{C}; H_\Gamma)$ is zero if and only if \mathbf{C} has full rank, i.e., rank L . The condition that \mathbf{C} is full rank can be formulated analogously to the argument for non-full-rank cycles in Equation (50), as follows:

$$\sum_{\ell \in [L/2]} (-\log \gamma_0^{(\ell)} + \log \gamma_1^{(\ell)} + \log \gamma_3^{(\ell)} - \log \gamma_2^{(\ell)}) = c_i \pmod{q-1},$$

for some $c_i \neq 0$.

Since this condition must hold for all $r \in [P]$, we can rewrite the expression in matrix-vector form:

$$\left(\begin{array}{c|c|c|c} -\hat{H}_Z^{(2,L)} & \hat{H}_Z^{(2,R)} & \hat{H}_Z^{(2,L)} & -\hat{H}_Z^{(2,R)} \end{array} \right) \log \underline{\gamma} = \underline{c} \pmod{q-1},$$

where \underline{c} is a vector with $c_i \neq 0$ for all $i \in [P]$. This establishes equation (21). Equation (22) can be derived in the same manner.

References

- [1] P. W. Shor, “Scheme for reducing decoherence in quantum computer memory,” *Phys. Rev. A*, vol. 52, no. 4, pp. 2493–2496, Oct. 1995.
- [2] A. M. Steane, “Error correcting codes in quantum theory,” *Physical Review Letters*, vol. 77, no. 5, p. 793, 1996.
- [3] D. Gottesman, “Stabilizer codes and quantum error correction,” Ph.D. dissertation, California Institute of Technology, May 1997.
- [4] A. Y. Kitaev, “Fault-tolerant quantum computation by anyons,” *Annals of Physics*, vol. 303, no. 1, pp. 2–30, 2003.
- [5] E. Dennis, A. Kitaev, A. Landahl, and J. Preskill, “Topological quantum memory,” *Journal of Mathematical Physics*, vol. 43, no. 9, pp. 4452–4505, 2002.
- [6] E. Knill and R. Laflamme, “Concatenated quantum codes,” *arXiv preprint quant-ph/9608012*, 1996.
- [7] A. G. Fowler, M. Mariantoni, J. M. Martinis, and A. N. Cleland, “Surface codes: Towards practical large-scale quantum computation,” *Physical Review A*, vol. 86, no. 3, p. 032324, 2012.
- [8] Google Quantum AI, “Suppressing quantum errors by scaling a surface code logical qubit,” *Nature*, vol. 614, no. 7949, pp. 676–681, 2023.
- [9] R. G. Gallager, “Low-density parity-check codes,” *Information Theory, IRE Transactions on*, vol. 8, no. 1, pp. 21–28, 1962.
- [10] D. J. MacKay and R. M. Neal, “Near shannon limit performance of low density parity check codes,” *Electronics letters*, vol. 32, no. 18, pp. 1645–1646, 1996.
- [11] T. J. Richardson, M. A. Shokrollahi, and R. L. Urbanke, “Design of capacity-approaching irregular low-density parity-check codes,” *IEEE Transactions on Information Theory*, vol. 47, no. 2, pp. 619–637, 2001.
- [12] D. J. MacKay, G. Mitchison, and P. L. McFadden, “Sparse-graph codes for quantum error correction,” *IEEE Transactions on Information Theory*, vol. 50, no. 10, pp. 2315–2330, 2004.

- [13] M. Hagiwara and H. Imai, “Quantum quasi-cyclic LDPC codes,” in *Proc. 2007 IEEE Int. Symp. Inf. Theory (ISIT)*, June 2007, pp. 806–810.
- [14] J.-P. Tillich and G. Zémor, “Quantum LDPC codes with positive rate and minimum distance proportional to the square root of the blocklength,” *IEEE Transactions on Information Theory*, vol. 60, no. 2, pp. 1193–1202, 2013.
- [15] P. Panteleev and G. Kalachev, “Asymptotically good quantum and locally testable classical LDPC codes,” in *Proceedings of the 54th Annual ACM SIGACT Symposium on Theory of Computing*, 2022, pp. 375–388.
- [16] M. B. Hastings, “Quantum codes from high-dimensional manifolds,” *Quantum*, vol. 5, p. 564, 2021.
- [17] N. P. Breuckmann and J. N. Eberhardt, “Balanced product quantum codes,” *IEEE Transactions on Information Theory*, vol. 67, no. 10, pp. 6653–6674, 2021.
- [18] D. J. C. MacKay, *Information Theory, Inference and Learning Algorithms*. Cambridge University Press, 2003.
- [19] T. Richardson and R. Urbanke, *Modern Coding Theory*. New York, NY, USA: Cambridge University Press, Mar. 2008.
- [20] J. Ezri, A. Montanari, and R. Urbane, “A generalization of the finite-length scaling approach beyond the bec,” in *2007 IEEE International Symposium on Information Theory*. IEEE, 2007, pp. 1011–1015.
- [21] M. P. Fossorier and S. Lin, “Soft-decision decoding of linear block codes based on ordered statistics,” *IEEE Transactions on information Theory*, vol. 41, no. 5, pp. 1379–1396, 2002.
- [22] P. Panteleev and G. Kalachev, “Degenerate quantum LDPC codes with good finite length performance,” *Quantum*, vol. 5, p. 585, 2021.
- [23] N. Raveendran and B. Vasić, “Trapping sets of quantum LDPC codes,” *Quantum*, vol. 5, p. 562, 2021.
- [24] D. Chytas, N. Raveendran, and B. Vasic, “Enhanced min-sum decoding of quantum codes using previous iteration dynamics,” *arXiv preprint arXiv:2501.05021*, 2025.
- [25] H. Yao, W. A. Laban, C. Häger, A. G. i Amat, and H. D. Pfister, “Belief propagation decoding of quantum LDPC codes with guided decimation,” in *2024 IEEE International Symposium on Information Theory (ISIT)*. IEEE, 2024, pp. 2478–2483.
- [26] S. Miao, J. Mandelbaum, H. Jäkel, and L. Schmalen, “A joint code and belief propagation decoder design for quantum LDPC codes,” in *2024 IEEE International Symposium on Information Theory (ISIT)*. IEEE, 2024, pp. 2263–2268.
- [27] M. Davey and D. MacKay, “Low-density parity check codes over $\text{GF}(q)$,” *IEEE Commun. Lett.*, vol. 2, no. 6, pp. 165–167, June 1998.
- [28] A. Bennatan and D. Burshtein, “Design of nonbinary LDPC codes for arbitrary discrete-memoryless channels,” *IEEE Transactions on Information Theory*, vol. 52, no. 2, pp. 549–583, 2006.
- [29] D. Declercq and M. Fossorier, “Decoding algorithms for nonbinary LDPC codes over $\text{GF}(q)$,” *IEEE Trans. Commun.*, vol. 55, no. 4, pp. 633–643, Apr. 2007.
- [30] K. Kasai, M. Hagiwara, H. Imai, and K. Sakaniwa, “Quantum error correction beyond the bounded distance decoding limit,” *IEEE Trans. Inf. Theory*, vol. 58, no. 2, pp. 1223–1230, 2012.
- [31] D. Komoto and K. Kasai, “Quantum error correction near the coding theoretical bound,” *arXiv:2412.21171*, 2024.
- [32] O. Ferraz, S. Subramanyan, R. Chinthalal, J. Andrade, J. R. Cavallaro, S. K. Nandy, V. Silva, X. Zhang, M. Purnaprajna, and G. Falcao, “A survey on high-throughput non-binary LDPC decoders: ASIC, FPGA, and GPU architectures,” *IEEE Communications Surveys and Tutorials*, vol. 24, no. 1, pp. 524–556, 2022.
- [33] Z. Liu and L. Zhao, “High-throughput software LDPC decoder on GPU,” *EURASIP Journal on Advances in Signal Processing*, vol. 2024, no. 1, p. 91, 2024.
- [34] K. Kasai, “Quantum error correction with girth-16 non-binary LDPC codes via affine permutation construction,” *arXiv:2504.17790*, 2025.
- [35] —, “Efficient Mitigation of Error Floors in Quantum Error Correction using Non-Binary Low-Density Parity-Check Codes,” *arXiv:2501.13923*, 2025, accepted for ISIT2025.
- [36] S. Myung, K. Yang, and D. S. Park, “A combining method of structured LDPC codes from affine permutation matrices,” in *2006 IEEE International Symposium on Information Theory*. IEEE, 2006, pp. 674–678.
- [37] R. Yoshida and K. Kasai, “Linear Permutation Polynomial Codes,” in *2019 IEEE International Symposium on Information Theory (ISIT)*, 2019, pp. 66–70.
- [38] M. Fossorier, “Quasicyclic low-density parity-check codes from circulant permutation matrices,” *IEEE Transactions on Information Theory*, vol. 50, no. 8, pp. 1788–1793, 2004.
- [39] A. R. Calderbank and P. W. Shor, “Good quantum error-correcting codes exist,” *Phys. Rev. A*, vol. 54, no. 2, pp. 1098–1105, Aug. 1996.
- [40] A. Steane, “Multiple-particle interference and quantum error correction,” *Proceedings of the Royal Society of London. Series A: Mathematical, Physical and Engineering Sciences*, vol. 452, no. 1954, pp. 2551–2577, 1996.
- [41] S. Lin, K. A. S. Abdel-Ghaffar, and D.-S. Rhee, “Structured low-density parity-check codes: Algebraic constructions,” in *Proc. IEEE Information Theory and Applications (ITA) Workshop*. IEEE, July 2004.
- [42] C. Di, T. Richardson, and R. Urbanke, “Weight distribution of low-density parity-check codes,” *IEEE Transactions on Information Theory*, vol. 52, no. 11, pp. 4839–4855, 2006.
- [43] F. J. MacWilliams and N. J. A. Sloane, *The Theory of Error-Correcting Codes*. Amsterdam: Elsevier, 1977.